NASA Technical Memorandum 102775

Laser Transit Anemometer Measurements on a Slender Cone in the Langley Unitary Plan Wind Tunnel

William M. Humphreys, Jr., William W. Hunter, Jr.,
Peter F. Covell, and Cecil E. Nichols, Jr.

December 1990

National Aeronautics and
Space Administration

Langley Research Center
Hampton, Virginia 23665-5225

Laser Transit Anemometer Measurements on a Slender Cone in the Langley Unitary Plan Wind Tunnel

SUMMARY

A Laser Transit Anemometry (LTA) system has been used to probe the boundary layer on a slender (5° half-angle) cone model in the Langley Unitary Plan Wind Tunnel. The anemometry system utilized a pair of laser beams with a diameter of 40 μm (0.0016 in.) spaced 1230 μm (0.0484 in.) apart to measure the transit times of ensembles of seeding particles using a cross-correlation technique. From these measurements boundary layer profiles around the model were constructed and compared with theory. The tunnel seeding system consisted of a small vibrated fluidized bed containing dry kaolin dust with a nominal particle size of 0.9 μm (3.54×10^{-5} in.). The kaolin was injected directly into the boundary layer via nine 1.32-mm (0.052-in.) orifices (three rows of three each) in the model nose. Dry kaolin dust was used as the seeding material to eliminate the problems of condensation present among seeding systems using liquid carriers such as ethanol.

The measured boundary layer profiles representing the boundary layer velocity normalized to the freestream as a function of height above the model surface were collected for zero angle of attack, Mach numbers of 2.5 and 4.5, and Reynolds numbers of 3.3×10^6 / meter and 6.6×10^6 / meter (1.0×10^6 / foot and 2.0×10^6 / foot) and were collected in a vertical plane that bisected the model's longitudinal center line at a location 635 mm (25 in.) from the tip of the forebody cone. The results indicated an excellent ability of the LTA system to make velocity measurements deep into the boundary layer. However, because of disturbances in the flow field caused by the onboard seeding system, premature transition to a turbulent boundary layer occured, implying that upstream seeding is mandatory if model flow field integrity is to be maintained.

INTRODUCTION

Programs such as the National AeroSpace Plane (NASP) are becoming increasingly dependent on having accurate flow diagnostic information in supersonic flows. Mie scattering-based laser anemometry, which utilizes a laser beam to nonintrusively probe the test medium, offers a method of measuring the flow velocity, flow angle, turbulence intensity, and shear stress around a test model under various flow conditions. Small probe volumes produce high laser power densities, allowing submicron seed particles to be used as the radiation scattering medium in the flow field as well as allowing measurements to be made very close to model surfaces (within $\approx$ 100 μm). In support of programs such as NASP, it was desired to demonstrate the usefulness of a Mie scattering-based system in the supersonic Langley Unitary Plan Wind Tunnel. To this end, an experiment was conducted using a Laser Transit Anemometry (LTA) system to probe the boundary layer on a slender (5° half angle) cone model at Mach numbers of 2.5 and 4.5. The specific goals of this test were:

1. Evaluate the general performance of laser velocimetry based on Mie scattering to achieve accurate velocity measurements in the facility.

2. Determine the most appropriate type and location of seeding system to use with the LTA system so that particle tracking is acceptable while at the same time ensuring that the flow field under investigation is not disturbed.

SYMBOLS

The units for the physical quantities in this paper are given both in U.S. Customary Units and in the International System of Units (SI). In the text the SI units will be given first with the U.S. Customary Units following in parentheses.

b	background noise estimate in time domain correlogram
C	contrast estimate for time domain correlogram
DT	delay time between adjacent bins of time domain correlogram function, sec
E_m	error in mean velocity estimate, m/sec (ft/sec)
E_s	error in velocity standard deviation estimate, m/sec (ft/sec)
excess	deviation of velocity space correlogram function from normal distribution
HW	half-width of self-adaptive triangular weighting filter
h	peak height of time domain correlogram function
m_k	k^{th} moment of velocity domain correlogram function
n	number of bins in correlogram function
$r(\tau_i)$	number of events in i^{th} channel of correlogram function in time domain
$r(\tau_i)'$	normalized number of events in i^{th} channel of correlogram function in time domain
$r(v_i)$	number of events in i^{th} channel of correlogram function in velocity domain
Q	total number of correlated events in time domain correlogram
q	total number of correlated events in velocity domain correlogram
$r_{a,b}$	individual channel data rates, pulses per sec
Re	unit Reynolds number per m (per ft)
s	beam separation, m (in.)
ST	integration time over which measurement is taken, sec

TI	measured turbulence intensity normalized to velocity magnitude at sample point in flow field
u	boundary layer local velocity, m/sec (ft/sec)
u_e	boundary layer edge velocity, m/sec (ft/sec)
V	measured mean flow velocity magnitude at sample point, m/sec (ft/sec)
v_i	i^{th} particle velocity measurement, m/sec (ft/sec)
$x(t_i)$	i^{th} pulse occurring on data channel a
$y(t_i)$	i^{th} pulse occurring on data channel b
x,y,z	model coordinates
z_f	focal depth of system, m (in.)
β	empirical filter constant (= 0.3)
Δz	height of sample volume above model surface, m (in.)
λ	laser wavelength, m (in.)
τ_i	i^{th} particle transit time between two beams, sec
ω_o	Gaussian waist radius of individual sample volume beam, m (in.)

DESCRIPTION OF EXPERIMENTAL APPARATUS

Laser Transit Anemometer (LTA)

In laser transit anemometry, the transit times of seed particles entrained in the flow field are measured as they cross the foci of a pair of parallel laser beams (Figure 1). The transit time of an individual particle, τ_i, in conjunction with the known beam separation, s, provides a measurement of the velocity, v_i, of the particle *in the plane normal to the optical axis of the system* by

$$v_i = \frac{s}{\tau_i} \tag{1}$$

Assuming that the particle faithfully tracks the flow field, v_i is a measure of the flow velocity in the measurement plane at the sample volume point. The beams are rotated about an axis that is equidistant from and parallel to the two beams. The ability to rotate the two beams allows for the determination of two dimensional flow angularity in the measurement plane.

The optics package used for this test was manufactured by Spectron Development Laboratories and is shown schematically in Figure 2. An argon-ion laser beam at a wavelength of 514.5 nm, circularly polarized, is sent through a Wollaston prism / lens assembly which splits the beam into a pair of parallel beams. These parallel beams are sent through a dove prism assembly mounted in a rotating ring controlled by a DC servo system to enable the two beams to be rotated precisely about a common optical axis. The beams then pass through a final field lens assembly and are focused to form two Gaussian waists at the measurement point in the flow. The system operates in a 180 degree backscatter mode with the scattered light from particles crossing the sample volume being collected around the annulus of the transmission optics. This scattered light passes through the dove prism assembly and beam stop (which blocks the focused image of each beam) and enters a fiber optic link connected to separate photomultiplier detectors. Each photomultiplier sends its output to a filter-discriminator / pulse-center detector circuit which produces a TTL level pulse whenever the signal exceeds a preset threshold level. Thus, as particles pass through the sample volume, a series of pulses are produced on two channels, each one corresponding to a separate beam.

The method used to extract transit time information for this test consists of computing the cross correlation function between the input pulse streams occurring on the two data channels. This discrete correlation function is given by

$$r(\tau_i) = \sum_{k=0}^{\infty} x(t_k)\, y(t_k + \tau_i) \qquad (2)$$

and is represented as a correlogram with 256 discrete channels or bins with each successive bin representing a delay time $\tau_i = i\Delta\tau$.

A block diagram of the LTA system used for this series of tests is shown in Figure 3. The LTA system is controlled by a MicroVAX II minicomputer system with 9 MB of main memory running at 0.9 MIPS. The computer is connected to an optical head controller which operates the image rotator as well as the discriminator / pulse-center detector circuits. The output from these detectors is sent to an event correlator which computes the cross correlation function in real time between the two channel data streams and relays this correlation function to the computer in the form of a correlogram which is a plot of the number of correlated events versus delay time, which is represented discretely in 256 channels or bins. LaRC-developed LTA data acquisition software manages all aspects of LTA system control and data acquisition as well as controlling the position of the scan rig containing the optics package. Figure 4 shows the LTA optics package mounted on the scan rig in front of test section 2 of the Langley Unitary Plan Tunnel.

Calibration of LTA System

The LTA focal point beam separation is a critical parameter, and any error in the measurement of this parameter directly affects system accuracy. The measurement of beam separation is performed by placing a 25-μm slit directly in front of a power meter detector at the focal point of the instrument. The focal length was approximately 900 mm for the optical

configuration used for this test. The slit/detector is aligned normal to the plane of the beams and scanned across both beams while monitoring laser power. A plot of laser power versus slit position allows the determination of both focal point beam diameter and beam separation. Using this technique, the beam diameter at the focal point was measured to be approximately 40 μm, while the beam separation was measured to be 1230 μm ± 10 μm. The depth of focus can be expressed using the Rayleigh range criteria [1] by:

$$z_r \approx \pm \frac{\pi \omega_o^2}{\lambda} \tag{3}$$

where z_r is the focal depth, ω_o is the beam radius, and λ is the laser wavelength. By using equation (3), the depth of focus for the instrument is computed as ± 2.44 mm. The active measurement volume is defined by the focal depth, beam separation, and beam waist cross section.

Wind Tunnel

The Langley Unitary Plan Wind Tunnel is a closed-circuit, continuous-flow, pressure tunnel with two 1.22- by 1.22- by 2.13-m (4- by 4- by 7-ft) test sections. The major elements of the facility are a 74.6-MW (100 000-hp) drive system, a dry air supply and evacuating system, a cooling system, and interconnecting ducting to produce the proper airflow through either of two test sections. The tunnel overall volume is 4642 m^3 (163,922 ft3). The tunnel circuit is designed to operate at pressure from near-vacuum to 10 atm (1 atm = 101.3 kPa). The settling chambers provide a large volume which results in low-velocity flow and smooth transition from the circular tunnel duct work to the rectangular nozzles and test section. The settling chamber for test section 2 used in this test is a cylindrical duct 3.66 m (12.0 ft) in diameter and 7.47 m (24.5 ft) long followed by a 1.07-m (3.5-ft) long transition section from circular to 1.22- by 2.67-m (4- by 8.75-ft) rectangular. The nozzle is of the asymmetric sliding-block type such that the nozzle throat-to-test-section area ratio can be varied to provide continuous variation of Mach number. With this arrangement, the Mach number in test section 2 is variable from 2.30 to 4.63 while the unit Reynolds number per m (per ft) is variable from 1.64 x 10^6 to 26.23 x 10^6 (0.50 x 10^6 to 8.00 x 10^6). [2]

Model

The model employed for this test consisted of a 5° half angle cone forebody, a cylindrical midbody, and a 9° truncated cone afterbody. Figure 5 gives the dimensions of these individual components making up the overall model. The model was attached to the model support system in test section 2 which provided for forward and aft travel of 0.921 m (36.25 in.) in the tunnel x direction and traverse travel of ±0.508 m (±20 in.) in the tunnel y direction. The model was maintained at a zero degree angle-of-attack. By traversing the LTA system on its scan rig while at the same time moving the model support system, approximately 80 percent of the model's surface was accessible for surveys. Figure 6 shows the mounted model in test section 2.

Seeding System

One of the challenges to using laser anemometry in supersonic facilities is the ability to introduce the proper type of seeding material into the flow field of interest without disturbing the flow. The seed material used must be sufficiently small that particulate flow field tracking error is acceptable to the researchers. Thus the choice of a proper seeding system and seed material constituted one of the goals of this test.

Several seeding systems were tried during the course of the experiments with varying degrees of success. The first two systems utilized polystyrene latex (PSL) microspheres, measured to be 0.6 μm (2.36×10^{-5} in.) in diameter, suspended in water and then suspended in pure ethanol. The PSL and liquid carriers were injected through six 0.64 mm (0.025 in.) orifices on the nose of the model, with the flow field across the orifices shearing off the liquid as it left, thus atomizing it. However, both systems were unsuccessful due to the incomplete atomization of the liquid carrier, causing the liquid to run down the sides of the model. The failure of the carrier to be atomized completely is due in part to the lower velocities present in the boundary layer of the model.

Due to these problems with using seeding materials in a liquid carrier, various dry seeding systems were investigated. The first dry seeding system consisted of injecting incense smoke through the same orifices on the model nose; however, the concentration of smoke was not sufficient to obtain good data rates with the LTA system. It was decided at this point to use dry kaolin [3] as the seeding material. A small vibrated fluidized bed (Figure 7) was used to create a cloud of dry kaolin particles which were injected into the flow via nine 1.32-mm (0.052-in.) orifices (three rows of three each) in the model nose (Figures 8 and 9). The kaolin used was Engelhard ASP 200 coated with 0.5 percent Degussa R972 to minimize caking and prevent agglomeration of particles. The nominal aerodynamic particle size of the kaolin was measured using a TSI model 3300 aerodynamic particle sizer to be 0.9 μm (3.54×10^{-5} in.), with 96 percent of the particles being less than or equal to 1.7 μm (6.69×10^{-5} in.) in diameter. A pressure differential of approximately 724.0 mm Hg (14 psi) was maintained across the fluidized bed during particle injection by leaving the intake of the seeding system at atmospheric pressure and allowing the low static pressure present in the tunnel provide the necessary pressure differential. Adequate data rates (greater than 1000 pulses/sec per channel) were obtained with the LTA system using this seeding arrangement.

LTA DATA ACQUISITION

The data acquisition procedure used for this series of tests allows the determination of mean velocity, mean flow angle, and the turbulence intensity along this angle. The basic procedure, illustrated in Figure 10, consists of collecting correlograms at between five and nine discrete angular positions preselected by the system operator. From this set of correlograms a measurement of the mean flow angle is made. Next, the beam orientation is set to the mean flow angle so that an additional correlogram containing the mean velocity and turbulence intensity information can be obtained.

Angular Search Procedure

For each correlogram obtained with the system, a contrast quantity defined [4] as

$$C \equiv \frac{h - b}{\sqrt{b}} \tag{4}$$

is computed, where h is the number of events occurring in the peak channel of the correlogram and b is the average level of background noise present in the correlogram (due to spurious correlations and flare light from model surfaces). A plot is produced of these contrast quantities versus angular position through which a least squares fit of a parabolic equation is performed. The abscissa of the parabolic vertex is taken to be the mean flow angle or best angle. Figure 11 shows an example of this process. The standard deviation of the least squares fit represents the error in the mean flow angle estimate. Once the mean flow angle is determined, the two beams are repositioned at this angle and a velocity magnitude measurement is performed. Note that this procedure assumes a constant particulate concentration present in the flow. If for some reason the particulate concentration should vary during data acquisition, the correlograms used to determine the mean flow angle can be normalized by

$$r(\tau_i)' = \frac{r(\tau_i)}{(\sqrt{r_a^2 + r_b^2})(ST)} \tag{5}$$

where $r(\tau_i)'$ is the number of events in the i^{th} channel of the normalized correlogram, $r(\tau_i)$ is the number of events in the i^{th} channel of the original correlogram, r_a, r_b are the individual data rates from each channel, and ST is the integration time over which the raw correlogram is collected. The normalized functions are then used in the least squares fit routine to determine the mean flow angle.

DATA ANALYSIS

Filtering and Noise Removal

The first step in the data analysis process (Figure 12) is the removal of noise from the correlogram through filtering and background removal. To filter the correlogram, a self-adaptive digital filter incorporating a Parzen triangular weighting function is used. The average background level for the function, b, is first estimated by averaging the correlogram between the third channel and the channel nearest to 0.6 times the peak channel. The total data in the correlogram, Q, is determined by adding up all the events in all the channels of the correlogram. The half-width of the filter is then computed by

$$HW = ROUND\left(\frac{\beta(Q - nb)}{2(h - b)}\right) \tag{6}$$

where the operation ROUND makes HW an integer. β is an empirical constant which provides control over the broadening induced by the filter while n is the number of bins in the correlogram (normally 256 for this instrument). For this series of tests, β was set to 0.3. Having computed HW, the filter is now used on the original correlogram. Each data point Y(k) in the function is replaced by a triangularly weighted average over the set of data points from locations k-HW to k + HW using

$$Y(k) \leftarrow \frac{1}{HW} \sum_{j=-HW}^{j=+HW} \left(1 - \frac{|k-j|}{HW}\right) Y(j) \qquad (7)$$

After filtering, a new estimate of the background noise is made by computing the average channel height over the first 20 percent of the bins in the correlogram and over the last 20 percent of bins. The greater of these two averages is then taken to be the background estimate which is then subtracted from the correlogram. Note that this background removal process assumes that the nonspurious correlations in the correlogram do not occupy more than the central 50 percent of the correlogram, thereby limiting the effective turbulence intensity that can be measured. Higher turbulence intensities can be measured, but an estimate of the background noise must be made by visual inspection of the correlogram and then subtracted out.

The final step in the noise removal process is to truncate the outliers to remove any stray background signals that remain beyond the bounds of the central correlogram distribution. The truncation limits are defined to be the channels on either side of the peak of the function which first fall below the average background estimate. The correlogram is zeroed out beyond these limits. Through visual inspection these truncation limits may be changed to correct failures in the automatic truncation limit algorithm due to unusual background features which sometimes appear in correlograms. An example of the noise reduction process can be seen in Figure 13 for a typical function.

Transformation to Velocity Space

Before the mean and higher order moments are extracted from the final correlogram acquired after the angle search, the nonlinearity between the time domain (also referred to as tau space) and velocity domain (or velocity space) must be taken into account. Note that this nonlinearity is a first order inverse relationship between time and velocity as represented by equation (1):

$$v_i = \frac{s}{\tau_i}$$

Before any flow parameters are extracted, the function is transformed from tau space to

velocity space through the application of the Jacobian function [5], τ^2/s, as shown below:

$$r(v_i) \leftarrow \frac{\tau_i^2}{s} r(\tau_i) \tag{8}$$

where $r(\tau_i)$ represents the number of events in the i^{th} discrete channel of the tau space correlogram and $r(v_i)$ is the number of events in the i^{th} discrete channel of the velocity space correlogram.

Extraction of Flow Parameters

For each correlogram transformed to velocity space, the total number of nonspurious correlated events in the correlogram is computed by

$$q = \sum_{i=0}^{n} r(v_i) \tag{9}$$

The mean velocity is computed by

$$V = \frac{\sum_{i=0}^{n} v_i \, r(v_i)}{q} , \tag{10}$$

while the higher-order moments are computed by

$$m_k = \frac{\sum_{i=0}^{n} (v_i - V)^k r(v_i)}{q} . \tag{11}$$

The turbulence intensity along the direction of the mean flow angle is defined as

$$T.I. = \frac{\sqrt{m_2}}{V} , \tag{12}$$

and is usually expressed as a percentage. The standard error in the mean velocity measurement can be determined from

$$Em = \frac{\sqrt{m_2}}{\sqrt{q}} , \tag{13}$$

while the standard error of the standard deviation can be determined from

$$Es = (\sqrt{m_2})(\frac{1}{\sqrt{2q}})(\sqrt{1 + \frac{excess}{2}}) , \tag{14}$$

where excess represents the deviation of the correlogram from a normal distribution and is defined as

$$excess = kurtosis - 3.0 = \frac{m_4}{(m_2)^2} - 3.0 \qquad (15)$$

Note that excess is zero for a purely normal distribution.

MEASUREMENT RESULTS

Boundary layer surveys were conducted in the vertical x-z plane at a longitudinal center line distance of 635 mm (25 in.) from the model apex. The surveys were obtained at free stream Mach numbers of 2.5 and 4.5 for Reynolds numbers of 3.3×10^6/m and 6.6×10^6/m (1.0×10^6/ft and 2.0×10^6/ft). Table I lists the LTA measured flow quantities as well as the tunnel free stream conditions for each measurement in the test. Each survey was started approximately 4-5 mm (0.157-0.197 in.) from the model surface. The two beams were lowered to the surface in discrete increments with a velocity measurement made at each step. Note that angles searches were not performed for these surveys because the flow angle was assumed to be parallel to the model surface over the range of profile measurement positions. Thus, the beams were oriented to be parallel to the model surface and only a single correlogram collected at each measurement point (see figure 10, alternate acquisition procedure). Data acquisition time was reduced by a factor of five to ten using this procedure.

The correlograms collected for the data points listed in Table I are shown in Figure 14, and several observations are in order. First, as the beams were lowered into the boundary layer, the measured turbulence intensity increased from a low value of 1.0 - 1.5 percent in the near free stream region to a high of 20.0 percent near the model surface. This effect can be seen in the turbulence intensity profiles shown in Figures 15-18. Second, the background noise rose steadily as the beams were lowered into the boundary layer. This effect, observed in similar tests, is not surprising given the increase in flare light as the model surface is approached. Finally, during the course of the surveys an occasional large surge would occur in the measured data rate and the correlogram would display unusual characteristics similar to the one shown in Figure 14 - File 21. At these times agglomerated particles were probably passing through the sample volume of the system.

An interesting effect observed from the collected correlograms is the nonsymmetric nature of the background noise present in many of the plots of Figure 14, especially for correlograms collected near the model surface. The background noise level is higher toward the longer transit time portions of the correlograms, corresponding to the lower velocity regions of the velocity space correlograms. The most likely cause of this effect is model vibrations during the tests. Such vibrations can cause integration of velocity regions in the boundary layer due to the finite size of the LTA sample volume. During the course of the tests, the model could be seen to vibrate several millimeters, especially with free stream Mach

numbers of 4.5. These vibrations can be reduced or eliminated with a stronger model support system.

VELOCITY PROFILES

Boundary layer velocity profiles corresponding to the measurements listed in Table I are shown in Figures 19-22. Also shown are theoretical predictions based on the method described in [6]. At Mach 2.5, the LTA data corresponds very nearly to the turbulent boundary layer prediction. While the LTA data at Mach 4.5 exhibits a turbulent boundary layer profile trend, it does not correspond as well with the turbulent prediction. Based on these comparisons, it is believed that the all the boundary layers are fully turbulent. The descrepancies between the LTA data and the theoretical turbulent boundary layer predictions are most likely due to the previously mentioned model vibration problems.

The development of a turbulent boundary layer condition on the model is not surprising even though the test Reynolds numbers were generally below previously measured cone transition Reynolds numbers. In [7], onset and end of transition Reynolds numbers of 11.5 x 10^6/m and 19.7 x 10^6/m (3.5 x 10^6/ft and 6.0 x 10^6/ft), respectively, were measured on a highly polished 10-degree cone. Several factors have likely contributed to premature transition at a lower Reynolds number in the present study. Foremost is the disturbance due to the ejection of seeding particles directly into the boundary layer. Shadowgraph photographs of the model during the course of the tests (Figure 23) show a shock at the seeding orifices on the model. Also, a slight buildup of kaolin was observed at the ejection orifices which would also contribute disturbances sufficient to create an observable weak shock even for the case of having the seeding system shut off. The disturbances caused by these two factors are sufficient to cause transition into a turbulent boundary layer. Obviously if upstream seeding were employed the direct disturbance to the boundary layer would be eliminated. However, due to the tendency of kaolin to stick on surfaces (the tunnel walls and model supports contained a dusting of kaolin, although this could have been caused by the proximity of the seeding orifices), it is still possible to disrupt the boundary layer even with upstream seeding due to the accumulation of kaolin on the model. It is also possible that surface roughness caused premature transition since the model was not highly polished.

Finally, note that in Figure 19, part of the LTA data was corrected. A height correction of 0.5 mm (1.969 x 10^{-2} in.) was necessary to remove a bias present in the scan rig readout of position due to mechanical errors early in the test.

CONCLUSIONS

The results of the surveys indicate that indeed Mie scattering-based laser velocimetry systems are capable of yielding significant flow information which would be difficult to obtain otherwise in the Unitary Plan wind tunnel. The area of greatest education from this test concerned the choice of which seeding method to use. It is obvious that onboard seeding as

was used to conduct this test has severe consequences in terms of obtaining accurate information about laminar boundary layers on models, due to the effect of premature transition from disturbances caused by injection of particles into the boundary layer. A more appropriate seeding system would consist of upstream injection of particles into the flow, preferably in the settling chamber of the tunnel. However, given the turbulent boundary layers present on the model, the LTA system performed adequately in surveying the boundary layer and was able to make measurements to within several microns of the model surface.

REFERENCES

1. Kingslake, R., Optical System Design, Academic Press, 1983.

2. Jackson, C.M. Jr., Corlett, W.A., and Monta, W.J., *Description and Calibration of the Langley Unitary Plan Wind Tunnel*, NASA TP-1905, 1981.

3. Patrick, W.P., *Overview of Solid Particle LV Seeding Techniques Used at United Technologies Research Center*, Proceedings of Workshop on Wind Tunnel Seeding Systems for Laser Velocimeters, NASA Conference Publication 2393, 1985.

4. Smart, A.E., and Mayo, W.T., *Techniques for the Measurement of Turbulence and High Speed Flow with a Laser Transit Anemometer*, AEDC Report TR-84-13, Volume 1, 1984.

5. Abbiss, J.B., *Laser Transit Anemometer Software Development Program*, NASA Contractor Report 4225, 1989.

6. Harris, J.E., and Blanchard, D.K., *Computer Program for Solving Laminar, Transitional, or Turbulent Compressible Boundary Layer Equations for Two-Dimensional and Axisymmetric Flow*, NASA TM-83207, 1982.

7. Fisher, D.F., and Dougherty, N.S., *Flight and Wind Tunnel Correlation of Boundary Layer Transition on the AEDC Transition Cone*, AGARD-CP-339, 1982.

TABLE I: LASER TRANSIT ANEMOMETER / VELOCITY PROFILE DATA

File #	Mach #	Re ($\times 10^6$)	Station (mm)	Δz (mm)	DT (nSec)	ST (sec)	V (m/s)	TI (%)	Em (m/s)	Es (m/s)
1	2.5	3.281	635.0	3.810	20.0	15.0	568.752	2.278	2.076	1.186
2	2.5	3.281	635.0	3.302	20.0	15.0	562.752	2.940	2.328	1.245
3	2.5	3.281	635.0	2.794	20.0	15.0	545.719	3.184	1.705	1.133
4	2.5	3.281	635.0	2.286	20.0	15.0	533.416	4.539	1.089	0.624
5	2.5	3.281	635.0	1.778	20.0	15.0	516.988	6.286	1.526	0.944
6	2.5	3.281	635.0	1.524	20.0	15.0	483.248	6.573	1.141	0.684
7	2.5	3.281	635.0	1.270	20.0	45.0	477.549	7.455	0.954	0.664
8	2.5	3.281	635.0	1.016	20.0	45.0	462.045	7.308	0.959	0.577
9	2.5	3.281	635.0	0.762	20.0	45.0	437.495	9.434	1.228	0.758
10	2.5	3.281	635.0	0.508	20.0	60.0	425.397	8.572	1.033	0.594
11	2.5	3.281	635.0	0.381	20.0	120.0	401.140	11.589	0.835	0.511
12	2.5	3.281	635.0	0.254	20.0	90.0	374.001	10.941	0.955	0.485
13	2.5	3.281	635.0	0.203	40.0	120.0	340.092	19.164	1.479	0.816
14	2.5	3.281	635.0	0.152	40.0	120.0	313.691	25.300	2.368	1.278
15	2.5	3.281	635.0	0.101	80.0	120.0	251.422	26.707	1.397	0.716
16	2.5	6.562	635.0	3.810	20.0	30.0	565.181	3.038	0.941	0.602
17	2.5	6.562	635.0	3.556	20.0	30.0	561.856	2.718	0.835	0.534
18	2.5	6.562	635.0	3.302	20.0	45.0	552.421	3.853	0.898	0.643
19	2.5	6.562	635.0	3.048	20.0	45.0	549.710	4.102	0.941	0.571
20	2.5	6.562	635.0	2.794	20.0	45.0	541.965	4.329	0.103	0.063
21	2.5	6.562	635.0	2.540	20.0	15.0	532.304	4.909	0.407	0.241
22	2.5	6.562	635.0	2.540	20.0	15.0	531.204	5.401	0.537	0.357
23	2.5	6.562	635.0	2.286	20.0	15.0	525.866	5.480	0.636	0.438
24	2.5	6.562	635.0	2.032	20.0	15.0	516.601	5.582	0.591	0.409
25	2.5	6.562	635.0	1.778	20.0	15.0	504.984	5.811	1.040	0.608
26	2.5	6.562	635.0	1.524	20.0	30.0	497.251	6.337	0.594	0.380
27	2.5	6.562	635.0	1.270	20.0	30.0	482.181	6.940	0.522	0.332
28	2.5	6.562	635.0	1.016	20.0	30.0	468.752	7.608	0.529	0.327
29	2.5	6.562	635.0	0.762	20.0	30.0	455.889	8.333	0.814	0.536
30	2.5	6.562	635.0	0.508	20.0	45.0	436.931	9.480	0.767	0.498
31	2.5	6.562	635.0	0.381	20.0	45.0	422.100	10.746	0.570	0.362
32	2.5	6.562	635.0	0.254	20.0	45.0	410.547	9.184	0.680	0.381
33	2.5	6.562	635.0	0.203	20.0	45.0	398.133	11.252	0.594	0.366
34	2.5	6.562	635.0	0.152	30.0	45.0	370.349	15.547	0.625	0.375
35	2.5	6.562	635.0	0.101	30.0	45.0	370.281	13.457	0.876	0.482
36	2.5	6.562	635.0	0.076	30.0	45.0	355.037	17.396	0.753	0.464
37	2.5	6.562	635.0	0.051	50.0	45.0	297.941	17.773	0.634	0.318
38	2.5	6.562	635.0	0.025	50.0	45.0	270.426	18.140	0.748	0.418
39	2.5	6.562	635.0	0.000	50.0	45.0	278.560	19.675	1.345	0.671

TABLE I: LASER TRANSIT ANEMOMETER / VELOCITY PROFILE DATA (continued)

File #	Mach #	Re ($\times 10^6$)	Station (mm)	Δz (mm)	DT (nSec)	ST (sec)	V (m/s)	TI (%)	Em (m/s)	Es (m/s)
40	4.5	3.281	635.0	25.197	15.0	45.0	717.521	0.995	0.626	0.397
41	4.5	3.281	635.0	12.497	15.0	30.0	716.339	1.409	0.350	0.285
42	4.5	3.281	635.0	10.719	15.0	30.0	716.967	1.295	0.301	0.222
43	4.5	3.281	635.0	8.687	15.0	45.0	717.106	1.339	0.263	0.211
44	4.5	3.281	635.0	7.671	15.0	45.0	713.839	1.497	0.294	0.230
45	4.5	3.281	635.0	6.655	15.0	45.0	708.565	1.881	0.379	0.300
46	4.5	3.281	635.0	5.639	15.0	45.0	699.933	2.417	0.524	0.350
47	4.5	3.281	635.0	5.131	15.0	45.0	695.977	2.869	0.587	0.493
48	4.5	3.281	635.0	4.623	15.0	45.0	691.445	3.012	0.609	0.494
49	4.5	3.281	635.0	4.115	15.0	45.0	688.220	2.917	0.637	0.404
50	4.5	3.281	635.0	3.607	15.0	45.0	676.592	3.686	0.776	0.493
51	4.5	3.281	635.0	3.353	15.0	30.0	672.760	3.736	0.890	0.650
52	4.5	3.281	635.0	3.099	15.0	30.0	672.153	3.655	0.969	0.621
53	4.5	3.281	635.0	2.845	15.0	30.0	666.495	4.418	1.127	0.728
54	4.5	3.281	635.0	2.591	15.0	45.0	660.700	4.661	0.990	0.666
55	4.5	3.281	635.0	2.337	15.0	45.0	652.134	5.252	1.219	0.971
56	4.5	3.281	635.0	2.083	15.0	30.0	634.794	6.521	0.507	0.374
57	4.5	3.281	635.0	1.829	15.0	30.0	627.016	6.498	0.508	0.340
58	4.5	3.281	635.0	1.575	15.0	30.0	616.266	7.836	0.616	0.467
59	4.5	3.281	635.0	1.321	15.0	30.0	602.075	8.986	0.678	0.512
60	4.5	3.281	635.0	1.067	15.0	30.0	590.480	9.678	0.735	0.514
61	4.5	3.281	635.0	0.813	15.0	30.0	570.035	11.010	0.828	0.522
62	4.5	3.281	635.0	0.559	20.0	30.0	528.058	15.686	1.051	0.654
63	4.5	3.281	635.0	0.305	20.0	45.0	485.752	17.544	1.063	0.634
64	4.5	3.281	635.0	0.178	25.0	90.0	455.226	21.879	1.735	1.039
65	4.5	3.281	635.0	0.153	25.0	90.0	492.119	22.748	3.487	1.756
66	4.5	6.562	635.0	127.229	15.0	30.0	728.464	1.168	0.204	0.178
67	4.5	6.562	635.0	101.829	15.0	30.0	731.463	1.359	0.730	0.483
68	4.5	6.562	635.0	76.429	15.0	30.0	725.633	1.261	0.653	0.474
69	4.5	6.562	635.0	51.029	15.0	30.0	724.081	1.281	0.399	0.322
70	4.5	6.562	635.0	38.329	15.0	30.0	720.012	1.079	0.181	0.154
71	4.5	6.562	635.0	33.249	15.0	30.0	720.644	1.164	0.669	0.392
72	4.5	6.562	635.0	25.629	15.0	15.0	720.607	1.131	0.448	0.354
73	4.5	6.562	635.0	25.527	15.0	30.0	719.776	1.260	0.155	0.132
74	4.5	6.562	635.0	25.197	15.0	30.0	720.537	1.246	0.134	0.119
75	4.5	6.562	635.0	12.929	15.0	30.0	718.677	1.115	0.166	0.140
76	4.5	6.562	635.0	12.827	15.0	30.0	719.886	1.192	0.093	0.080
77	4.5	6.562	635.0	4.039	15.0	30.0	700.248	2.647	0.513	0.459
78	4.5	6.562	635.0	3.937	15.0	30.0	691.828	3.272	0.354	0.299

TABLE I: LASER TRANSIT ANEMOMETER / VELOCITY PROFILE DATA (concluded)

File #	Mach #	Re ($\times 10^6$)	Station (mm)	Δz (mm)	DT (nSec)	ST (sec)	V (m/s)	TI (%)	Em (m/s)	Es (m/s)
79	4.5	6.562	635.0	3.683	15.0	30.0	687.612	3.554	0.413	0.345
80	4.5	6.562	635.0	3.429	15.0	30.0	680.531	4.058	0.510	0.377
81	4.5	6.562	635.0	3.023	15.0	30.0	678.065	4.279	0.647	0.529
82	4.5	6.562	635.0	2.921	15.0	30.0	668.234	4.593	0.642	0.487
83	4.5	6.562	635.0	2.413	15.0	30.0	656.287	5.285	0.168	0.113
84	4.5	6.562	635.0	2.007	15.0	30.0	652.655	5.237	0.935	0.619
85	4.5	6.562	635.0	1.905	15.0	45.0	643.759	5.948	0.859	0.553
86	4.5	6.562	635.0	1.397	15.0	45.0	624.856	7.516	1.149	0.767
87	4.5	6.562	635.0	1.143	15.0	60.0	617.518	8.101	1.162	0.821
88	4.5	6.562	635.0	0.991	15.0	60.0	614.507	8.211	1.156	0.865
89	4.5	6.562	635.0	0.889	15.0	60.0	594.956	9.852	1.394	0.925
90	4.5	6.562	635.0	0.737	20.0	60.0	600.653	9.885	1.451	1.061
91	4.5	6.562	635.0	0.635	20.0	90.0	583.029	10.343	1.251	0.721
92	4.5	6.562	635.0	0.610	20.0	90.0	594.032	9.750	1.185	0.831
93	4.5	6.562	635.0	0.508	20.0	90.0	562.409	12.881	1.564	0.912
94	4.5	6.562	635.0	0.483	20.0	90.0	578.755	11.251	1.356	0.923
95	4.5	6.562	635.0	0.432	20.0	90.0	577.000	11.824	1.463	0.979
96	4.5	6.562	635.0	0.381	20.0	90.0	564.924	12.629	1.544	1.022
97	4.5	6.562	635.0	0.330	20.0	90.0	555.855	13.320	1.642	1.065
98	4.5	6.562	635.0	0.280	20.0	90.0	555.539	14.010	1.810	1.254
99	4.5	6.562	635.0	0.254	20.0	90.0	556.784	13.149	1.731	1.161
100	4.5	6.562	635.0	0.229	20.0	90.0	545.558	15.418	1.895	1.253
101	4.5	6.562	635.0	0.203	20.0	90.0	535.187	15.448	1.928	1.260
102	4.5	6.562	635.0	0.178	20.0	90.0	532.287	15.478	1.924	1.199
103	4.5	6.562	635.0	0.153	20.0	90.0	535.557	15.116	1.926	1.148
104	4.5	6.562	635.0	0.127	20.0	90.0	537.788	14.076	1.895	1.124
105	4.5	6.562	635.0	0.102	20.0	90.0	527.429	15.298	1.937	1.167
106	4.5	6.562	635.0	0.076	20.0	90.0	526.443	14.855	1.994	1.144
107	4.5	6.562	635.0	0.051	20.0	90.0	508.580	18.251	2.392	1.418
108	4.5	6.562	635.0	0.026	20.0	90.0	501.819	18.316	2.345	1.405
109	4.5	6.562	635.0	0.000	20.0	90.0	514.103	17.297	2.465	1.395

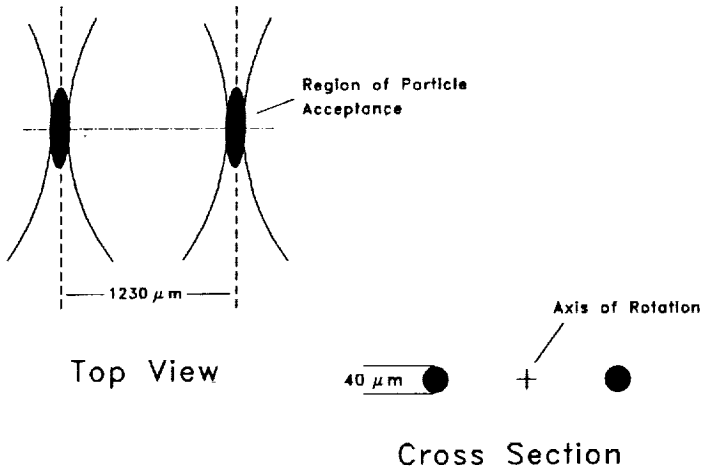

Figure 1: LTA Sample Volume Geometry

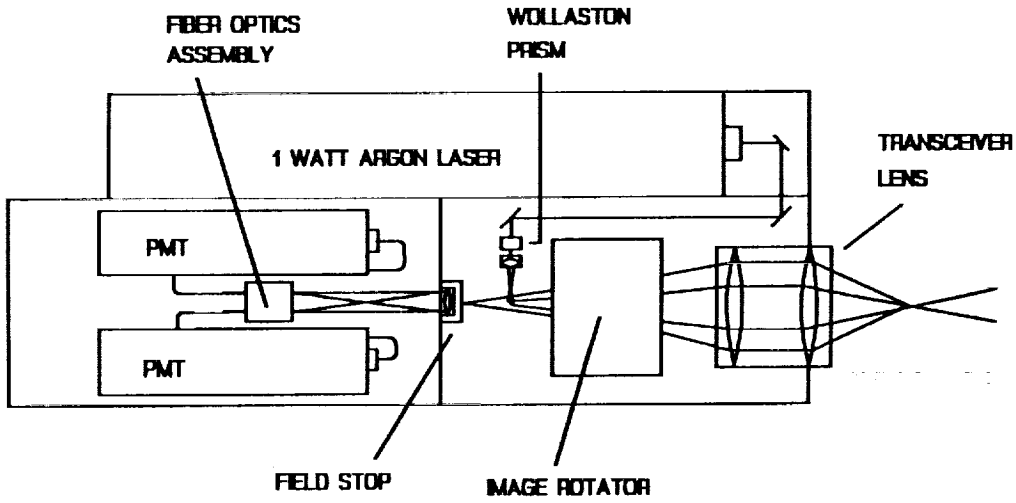

Figure 2: LTA Optical Head Schematics

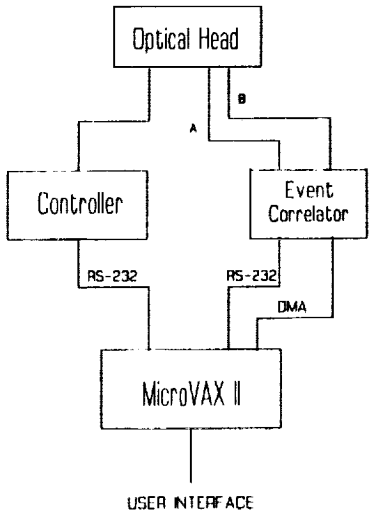

Figure 3: Block Diagram of LTA Hardware

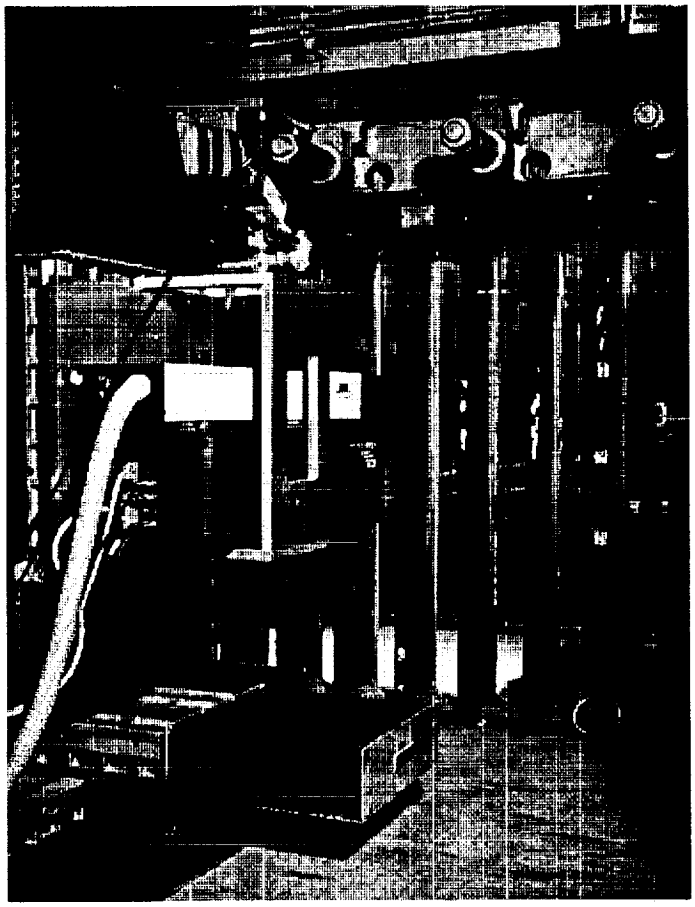

Figure 4: Laser Transit Anemometer System Mounted on Scan Rig

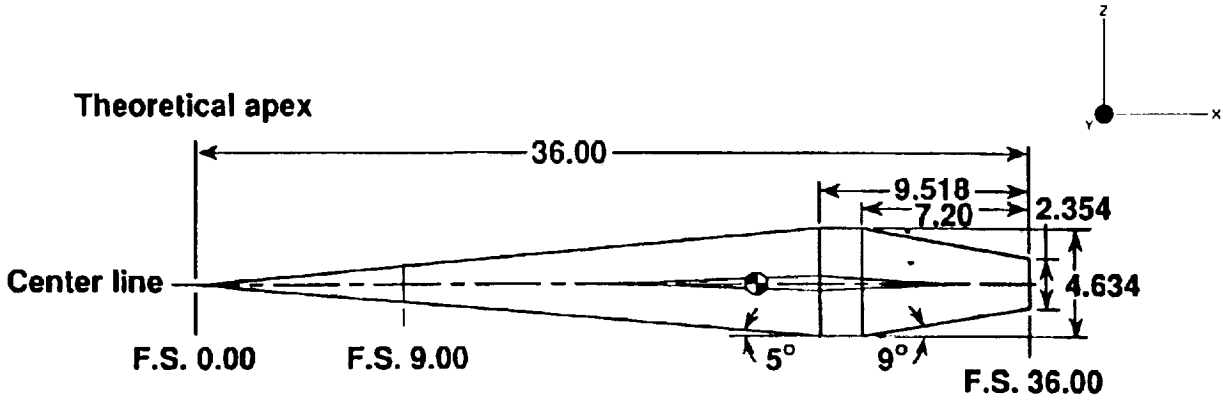

Figure 5: Geometric Description of Model (in inches)

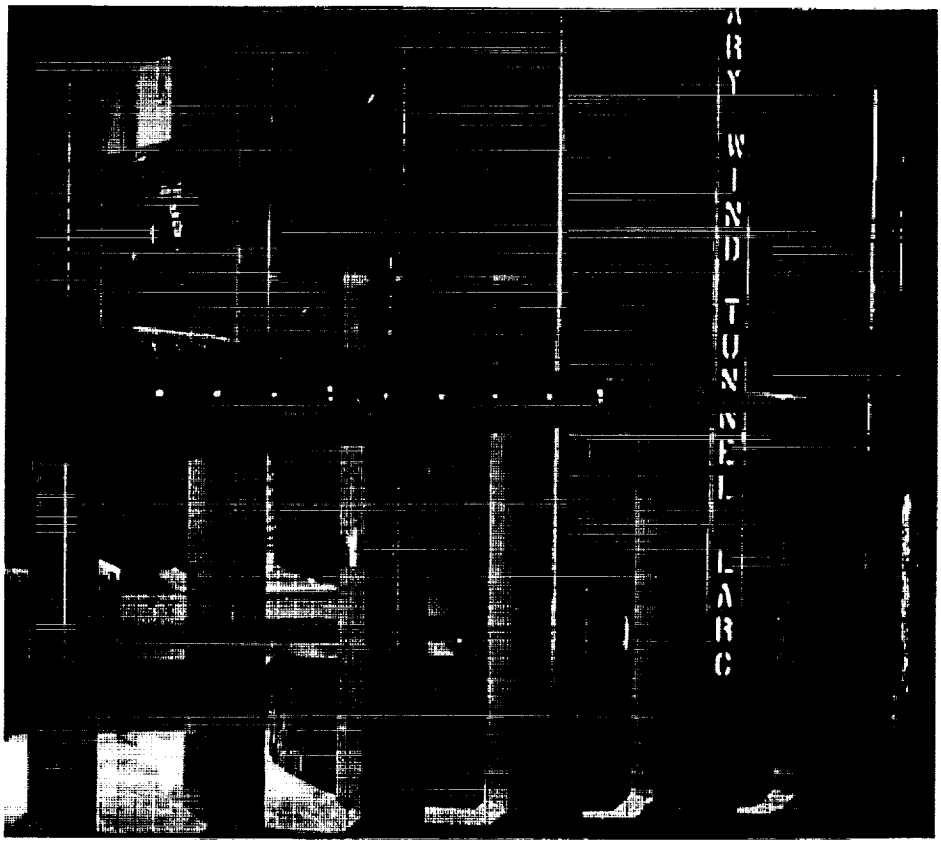

Figure 6: Mounted Model in Test Section 2

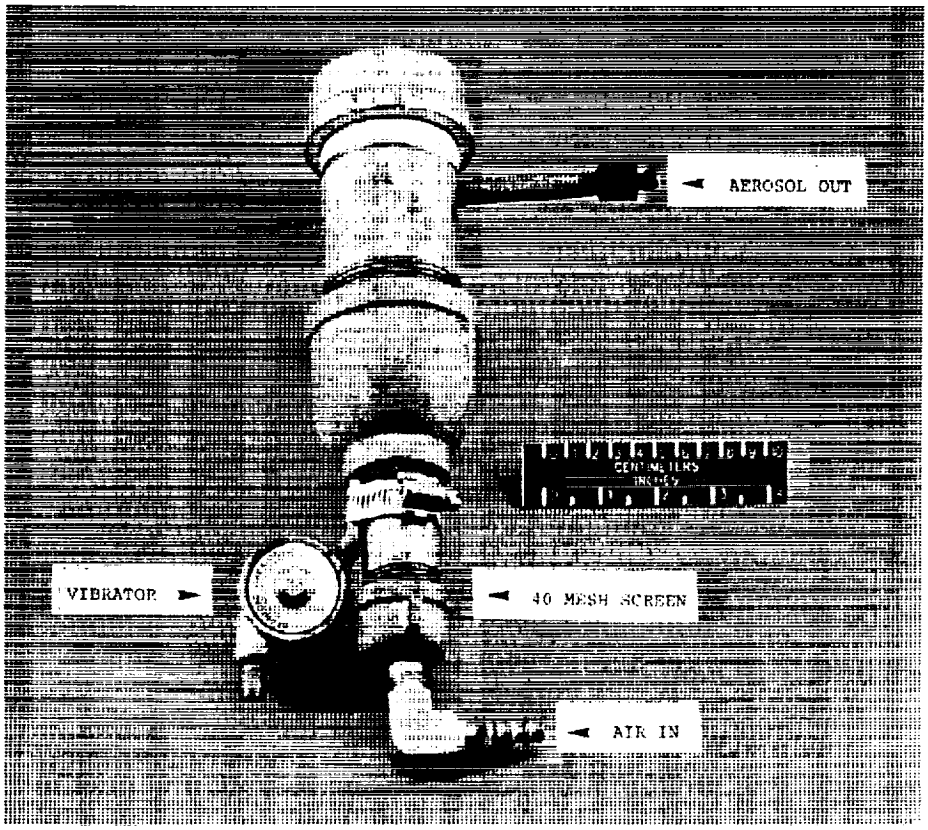

Figure 7: Close-up Photo of Vibrated Bed Seeding System

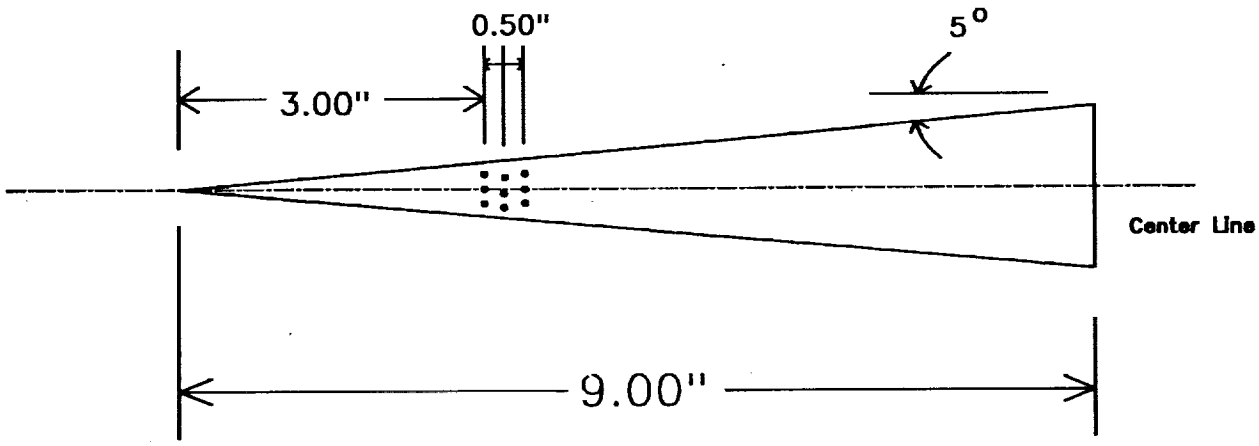

Figure 8: Orifice Geometry (in inches)

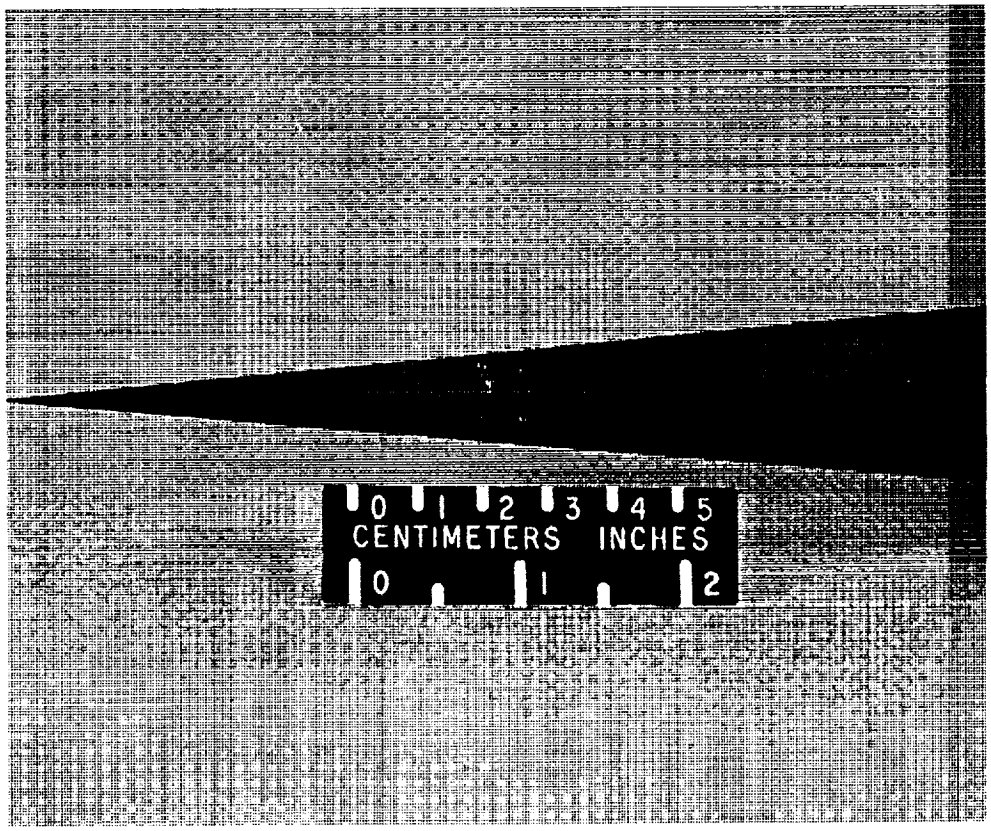

Figure 9: Close-up Photo of Orifice Configuration on Model

ORIGINAL PAGE
BLACK AND WHITE PHOTOGRAPH

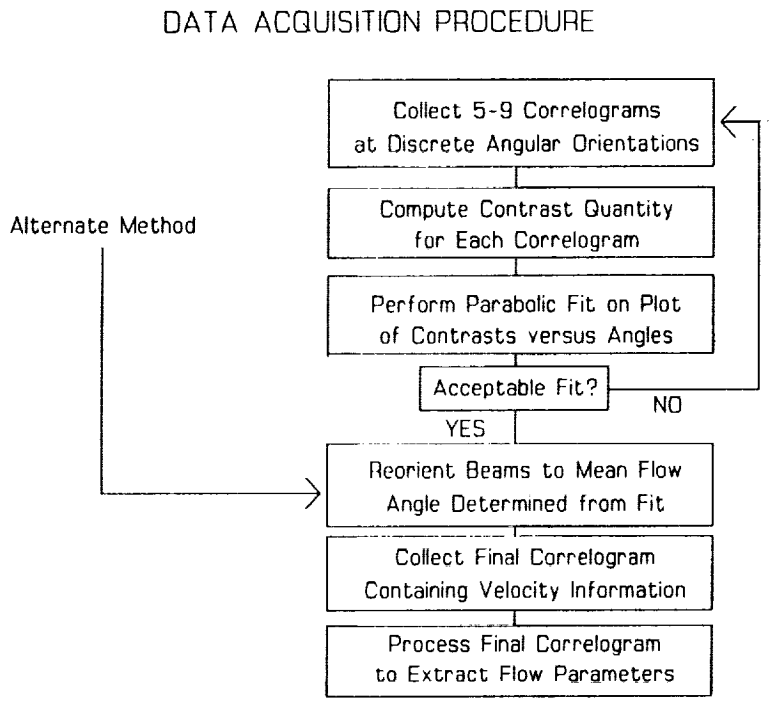

Figure 10: Laser Transit Anemometer Data Acquisition Procedure

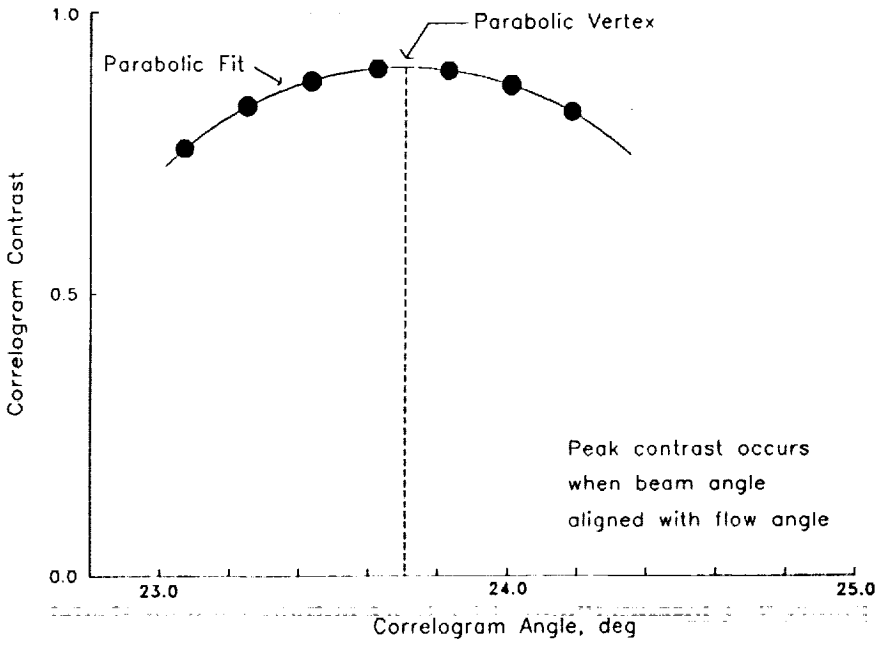

Figure 11: Parabolic Fit Procedure for Determining Mean Flow Angle

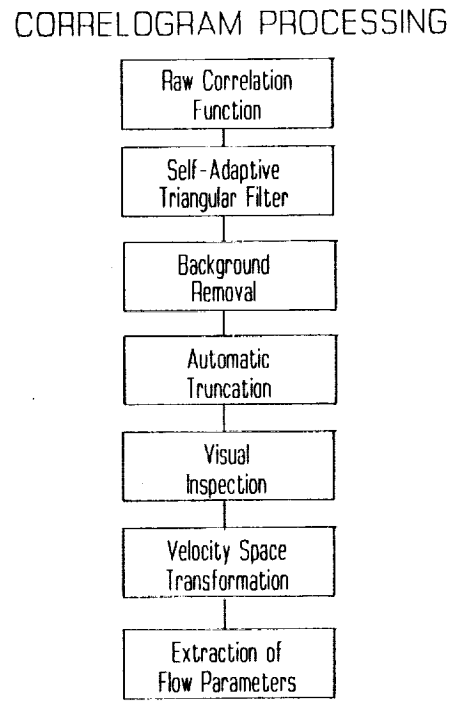

Figure 12: Laser Transit Anemometer Data Analysis Procedure

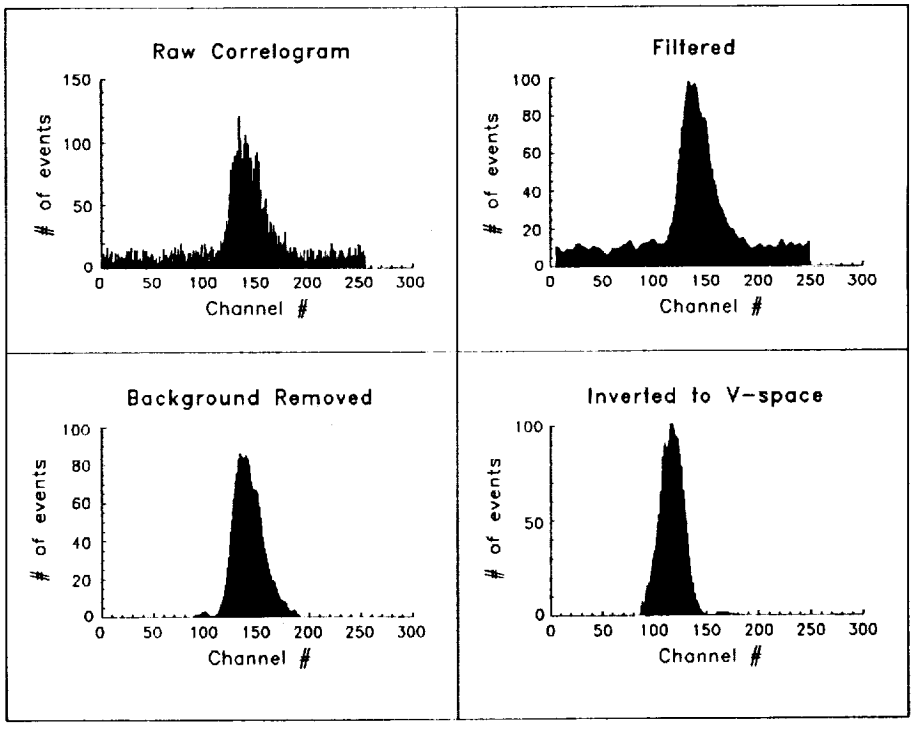

Figure 13: Example of Laser Transit Anemometer Data Processing Sequence

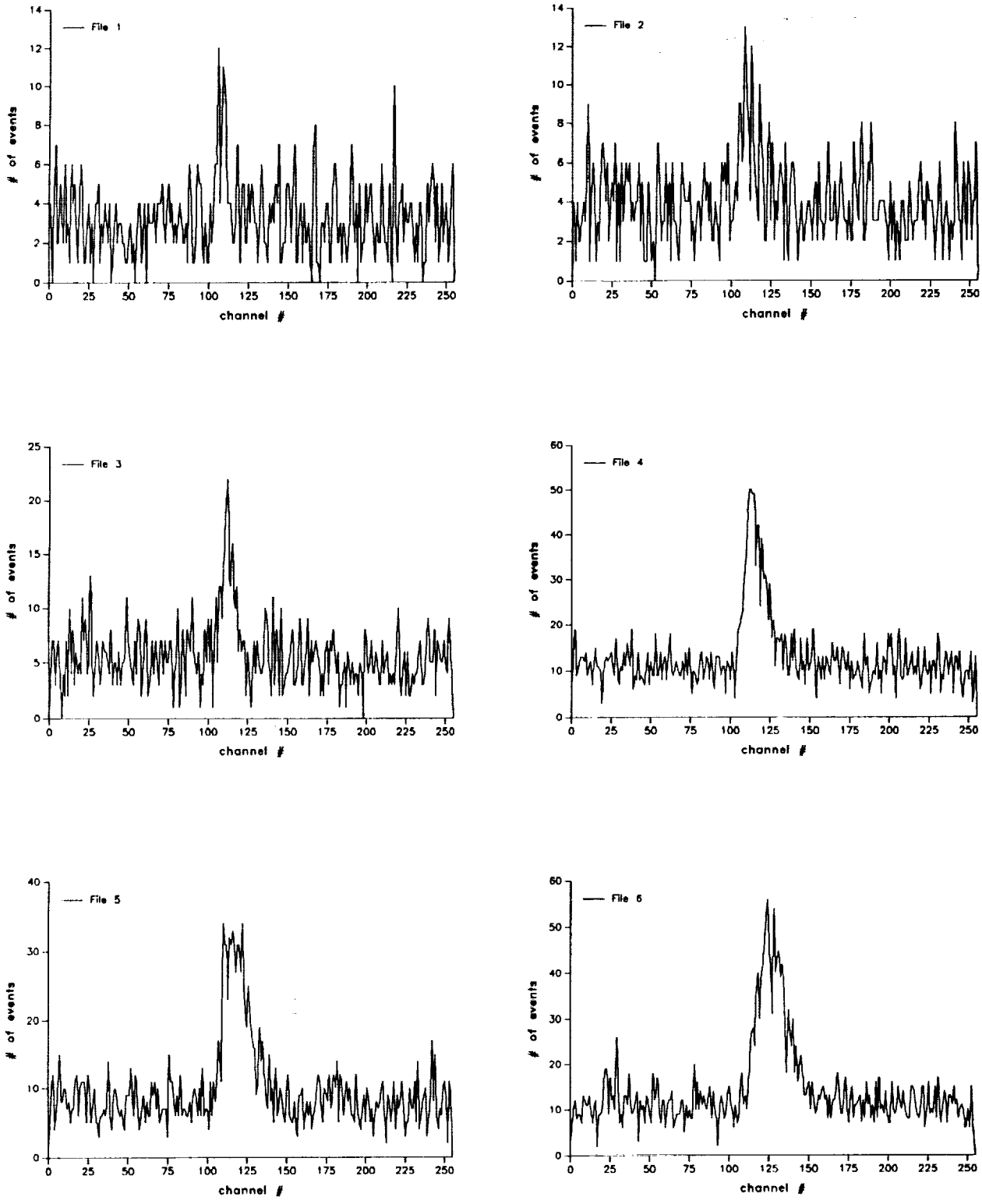

Figure 14: Correlogram Plots for Entries in Table I

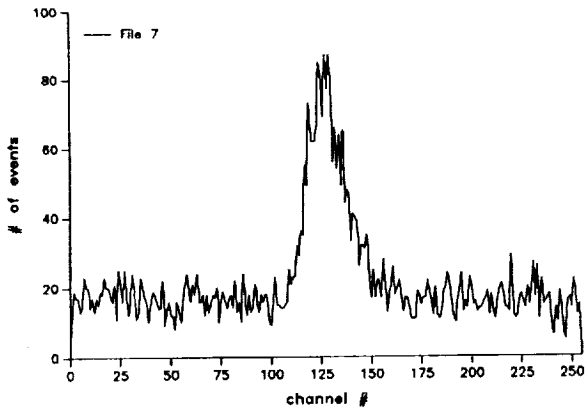

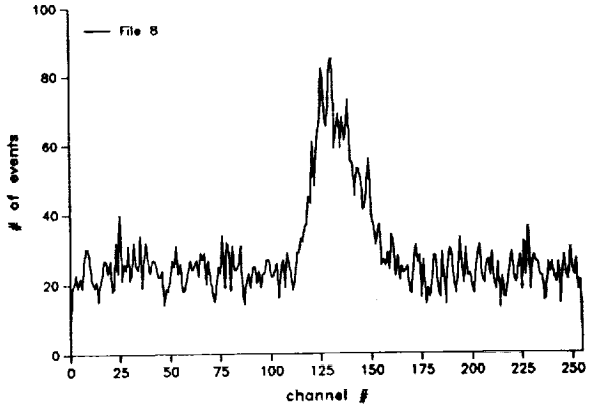

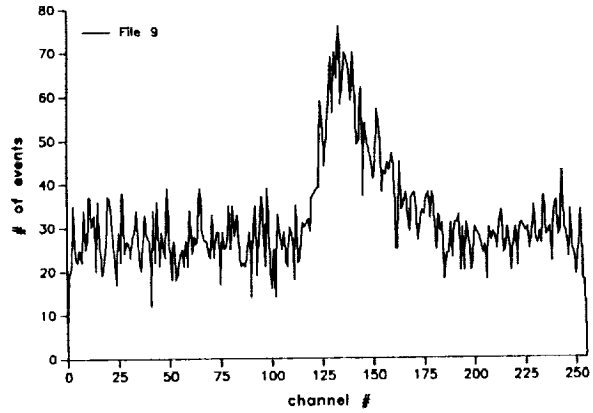

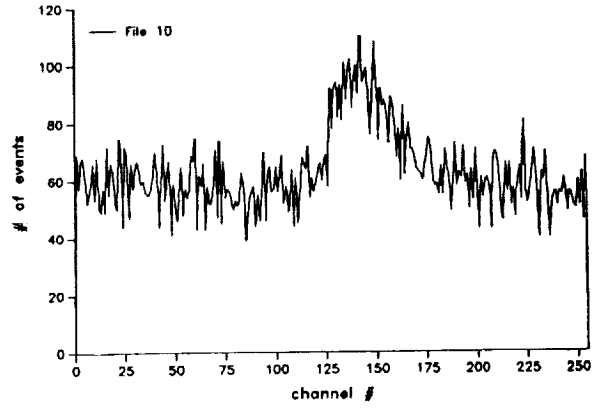

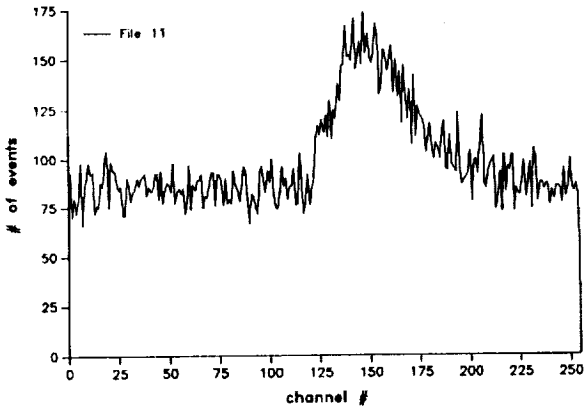

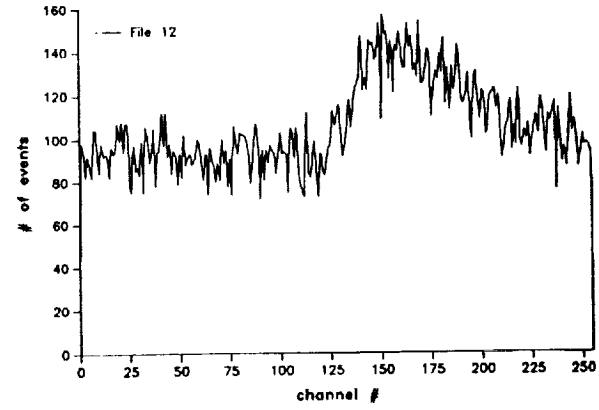

Figure 14: Continued

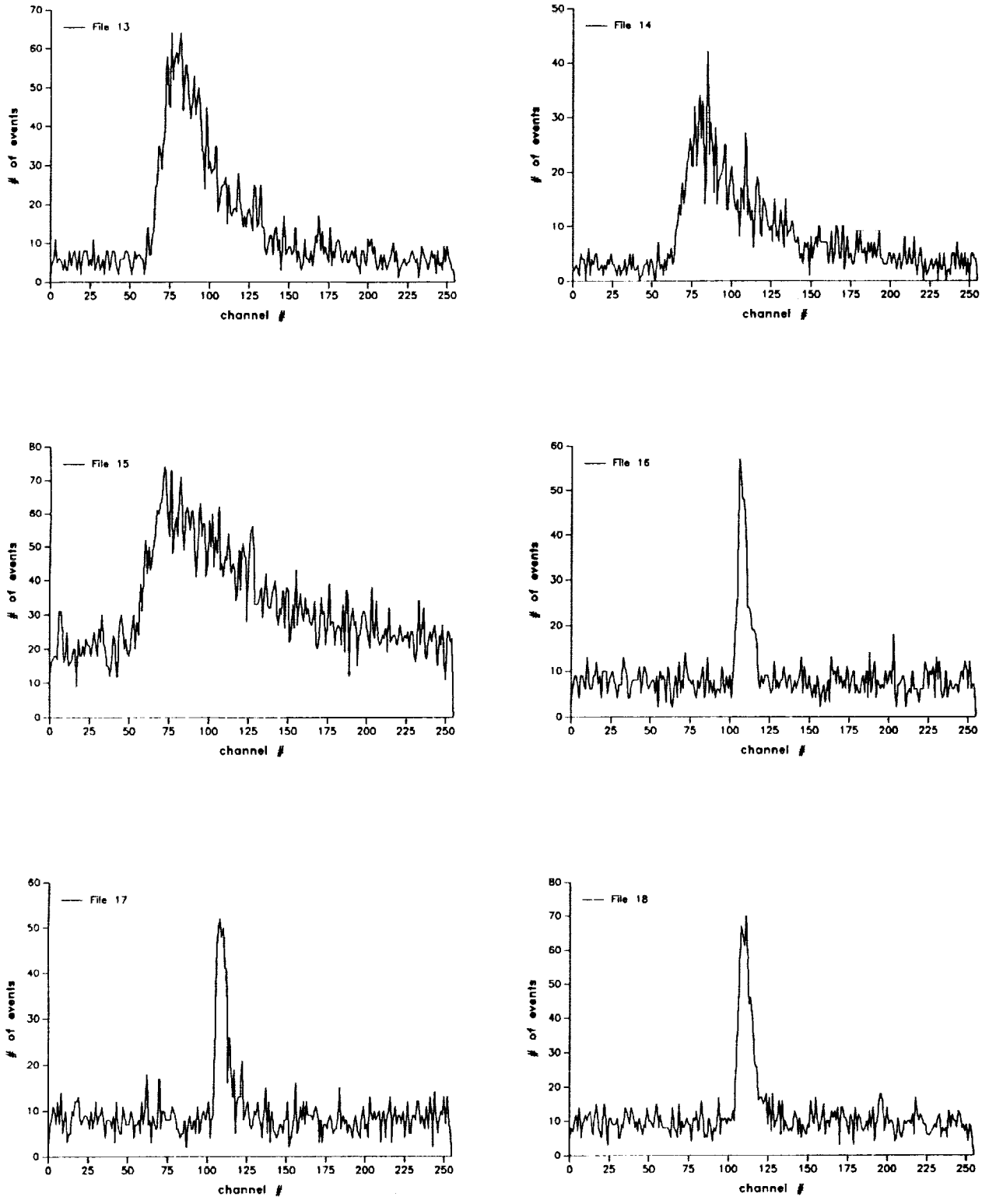

Figure 14: Continued

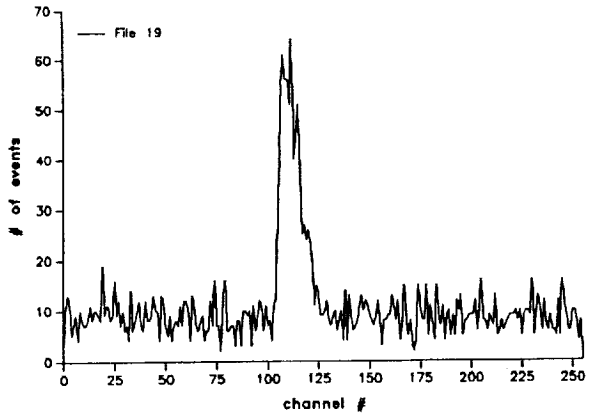

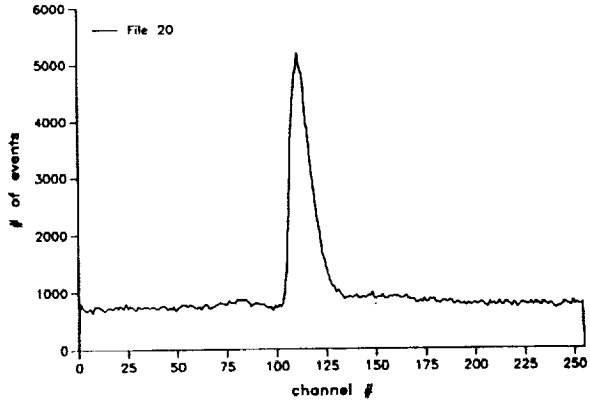

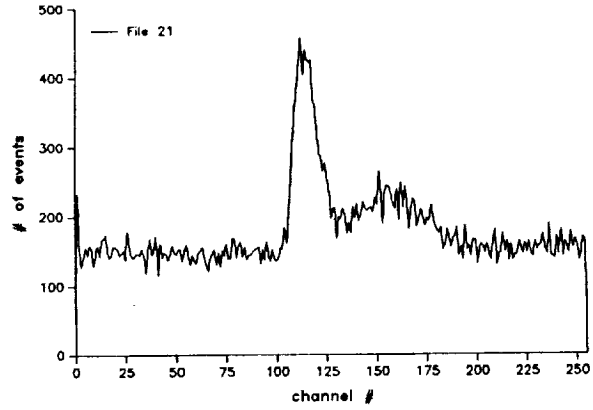

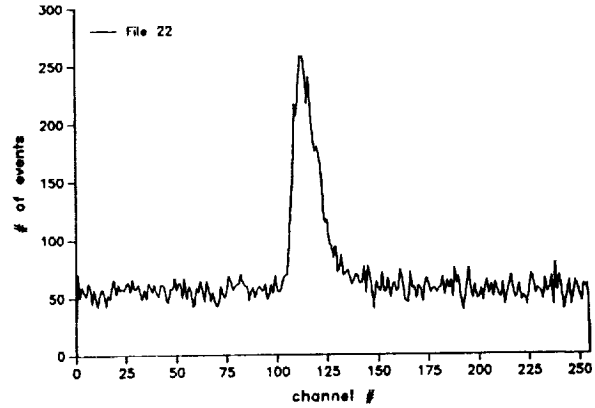

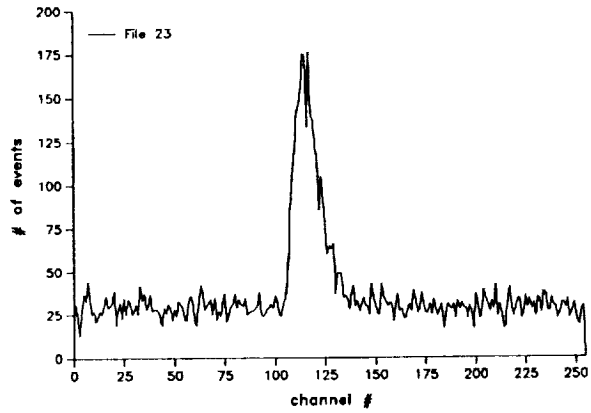

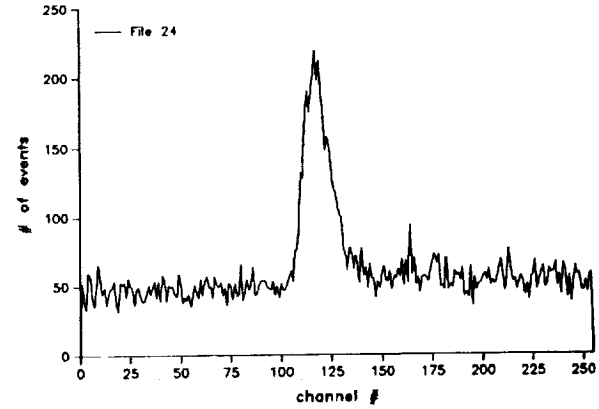

Figure 14: Continued

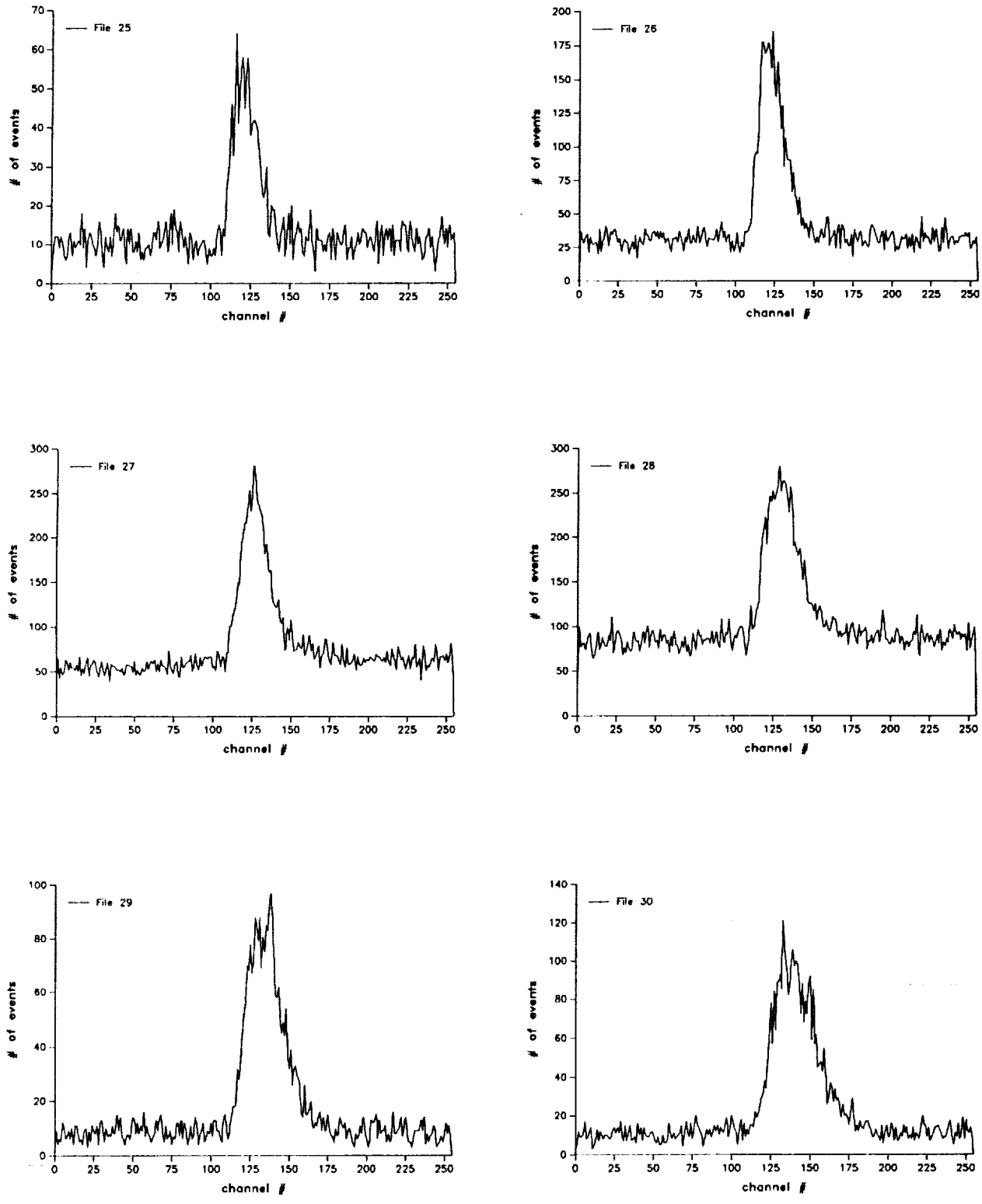

Figure 14: Continued

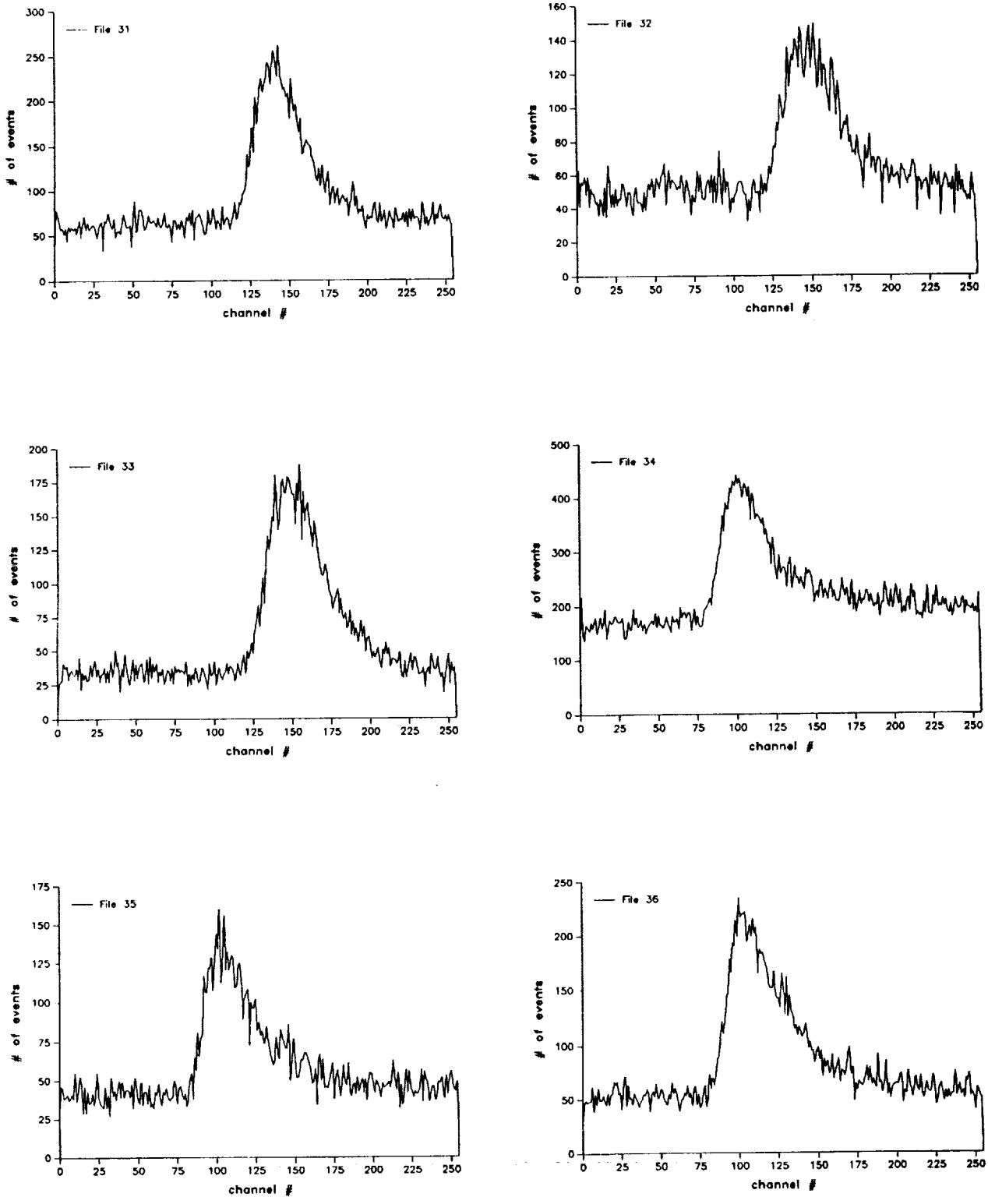

Figure 14: Continued

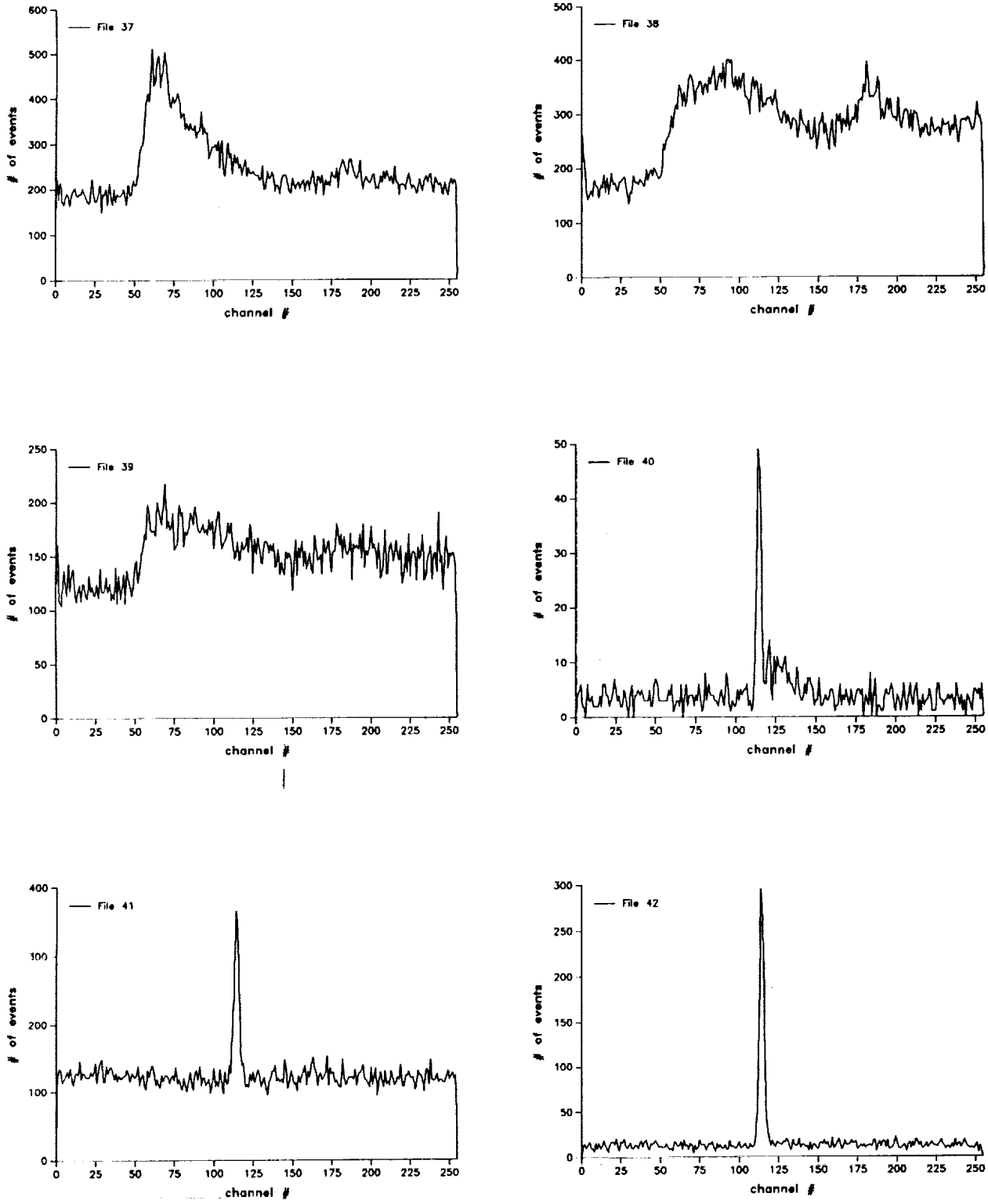

Figure 14: Continued

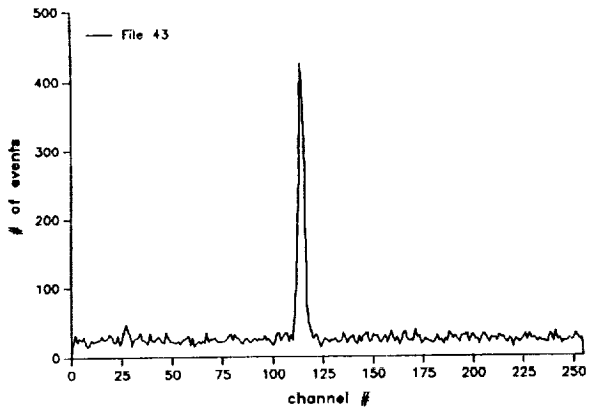

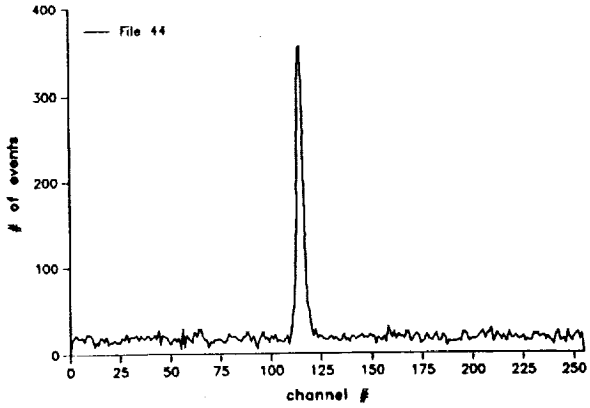

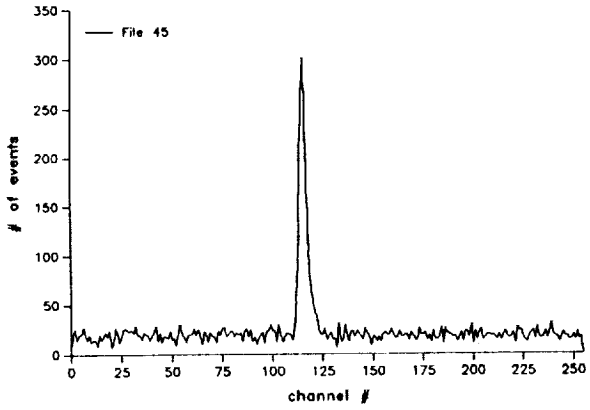

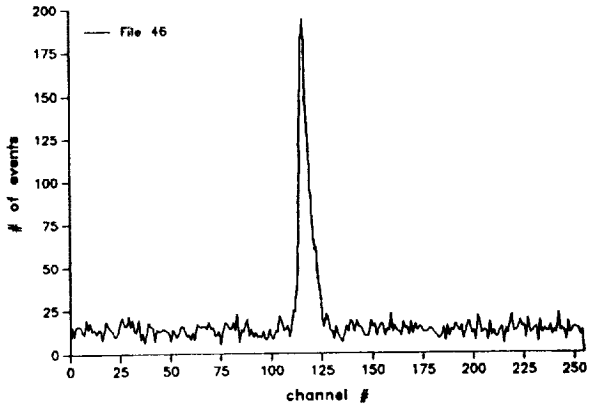

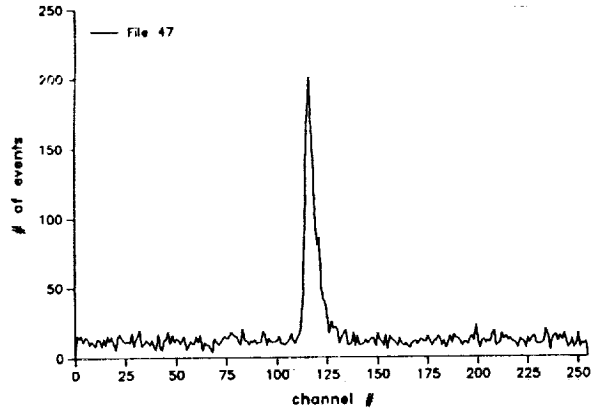

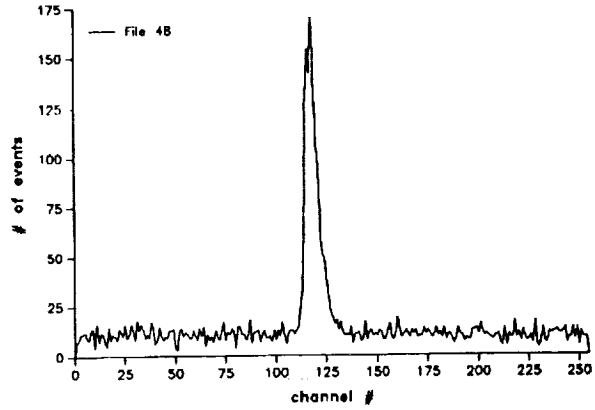

Figure 14: Continued

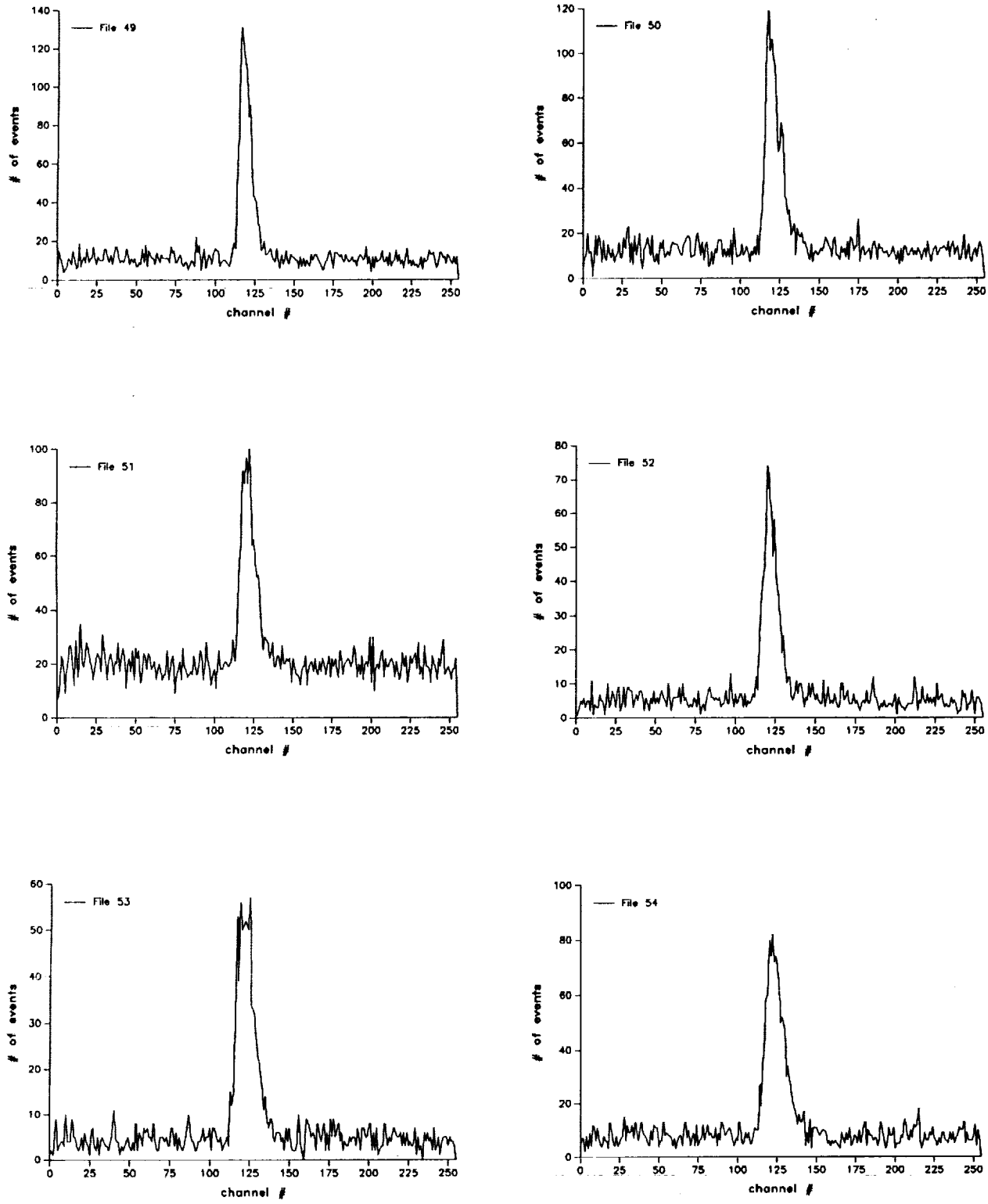

Figure 14: Continued

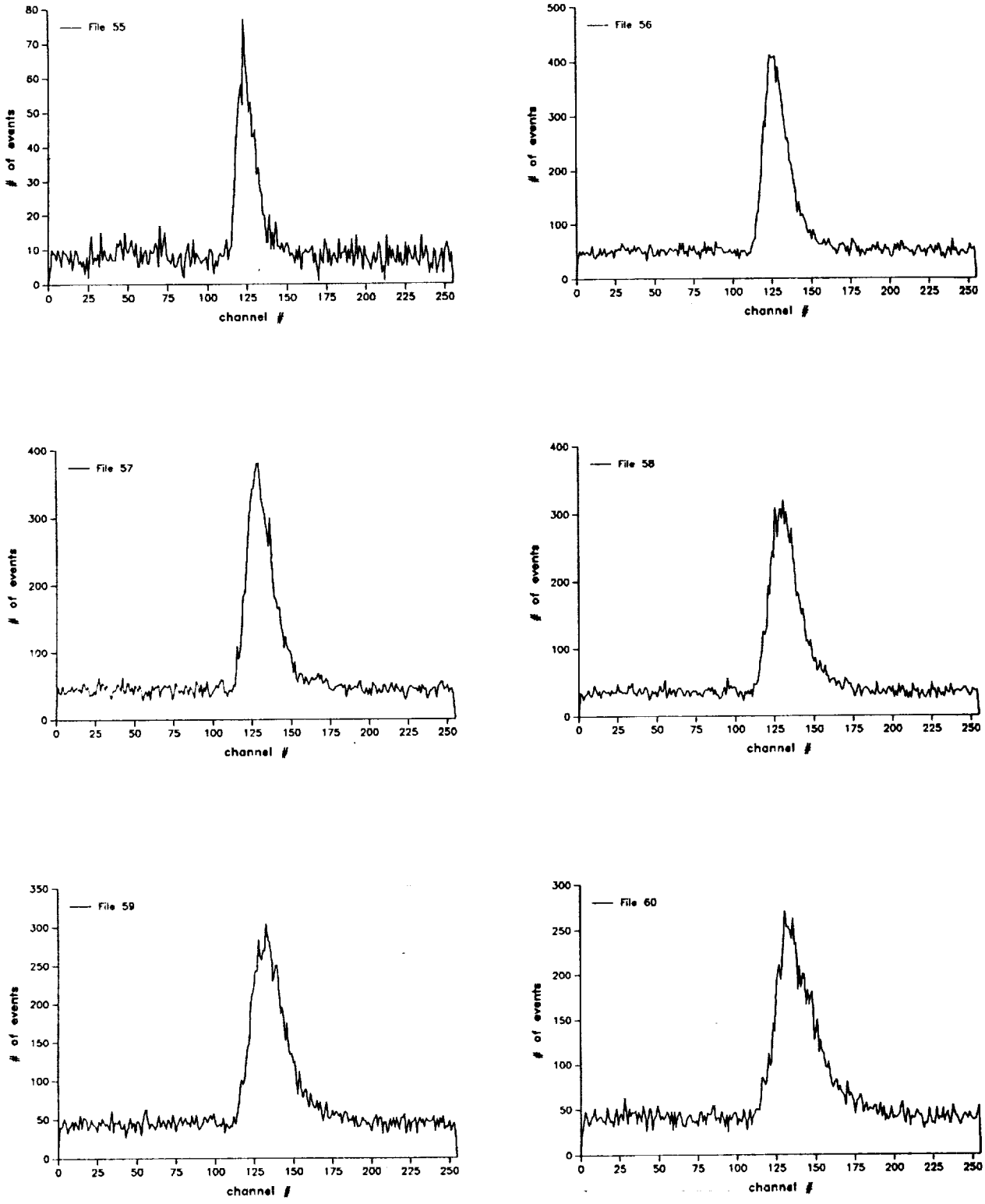

Figure 14: Continued

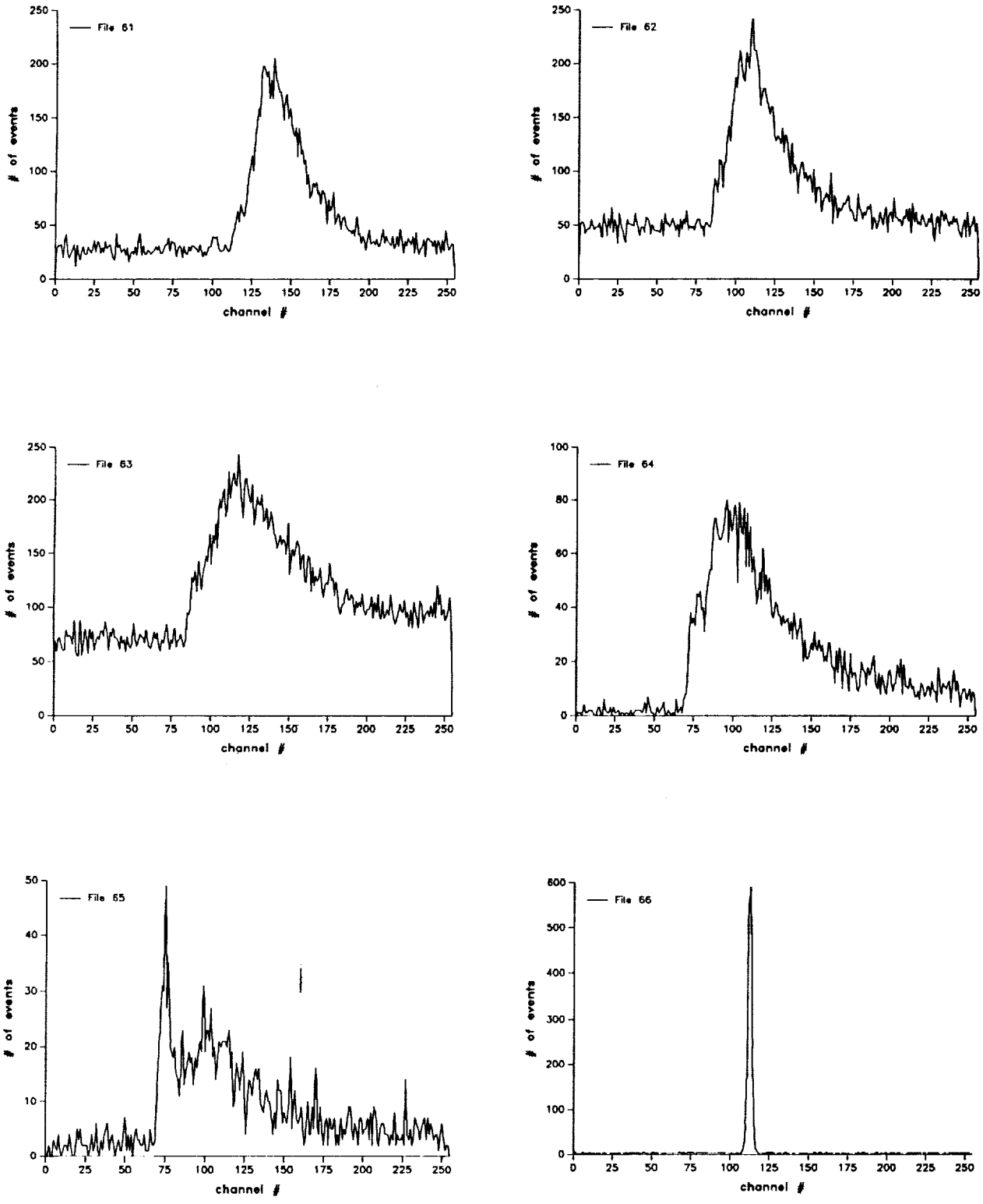

Figure 14: Continued

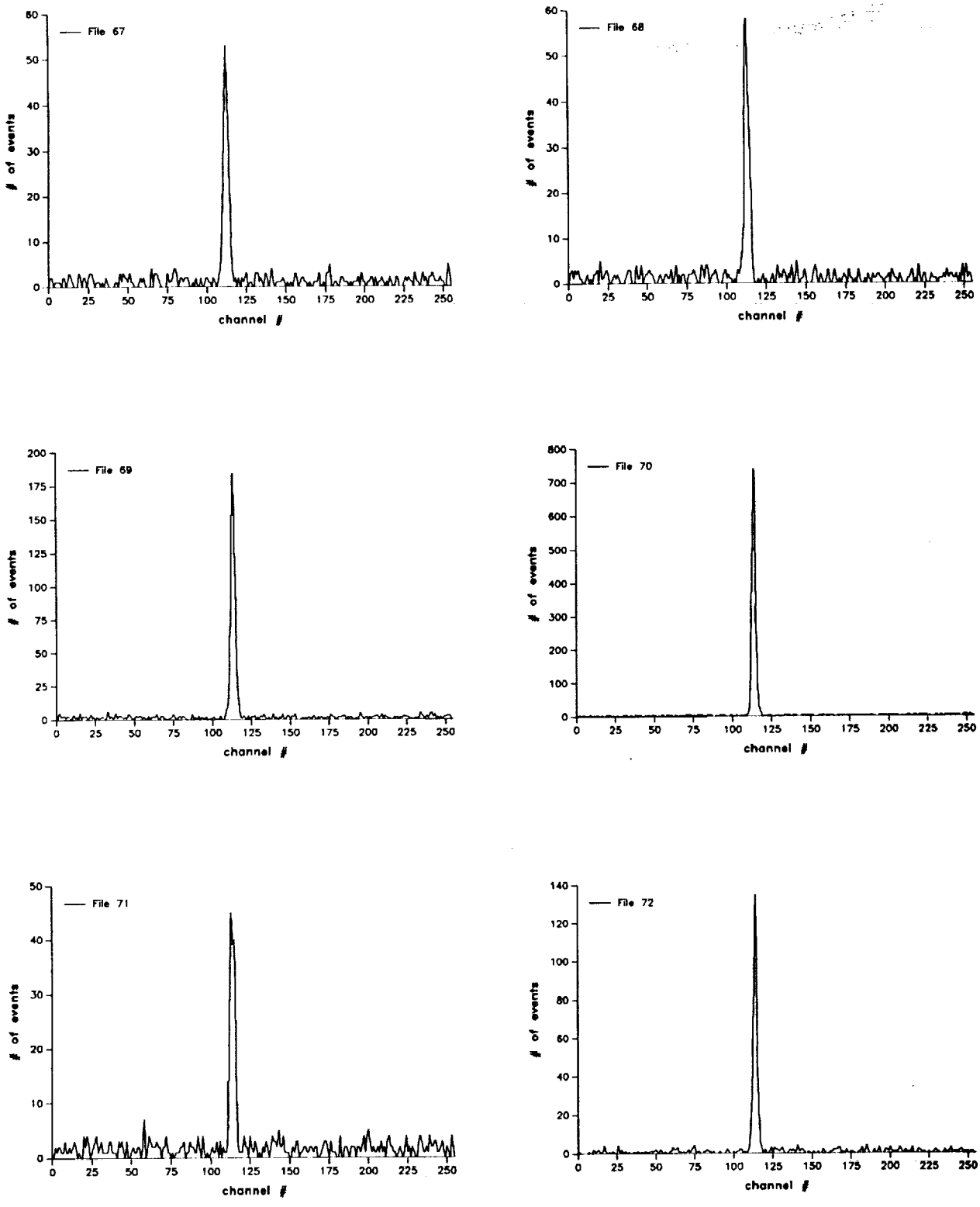

Figure 14: Continued

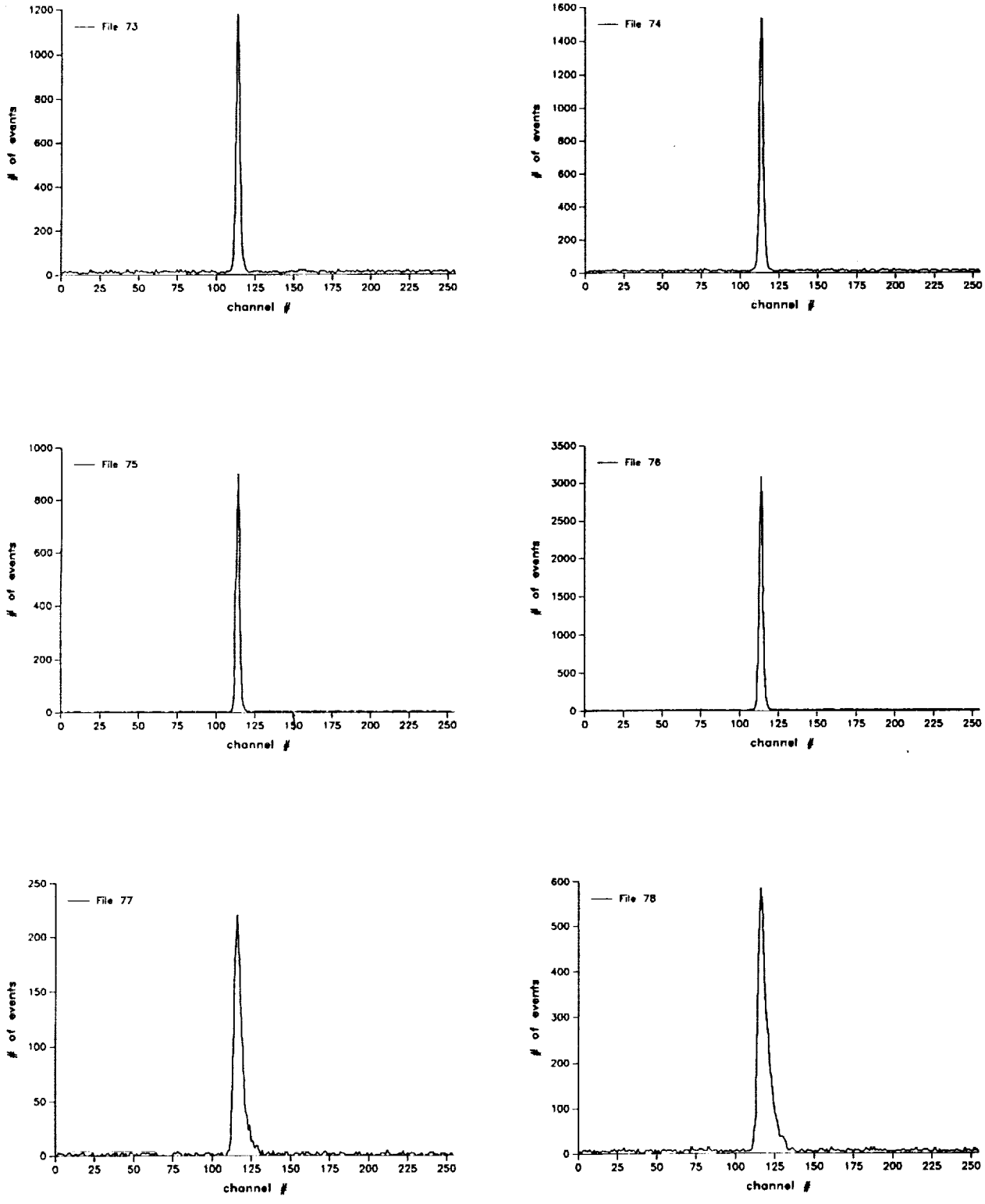

Figure 14: Continued

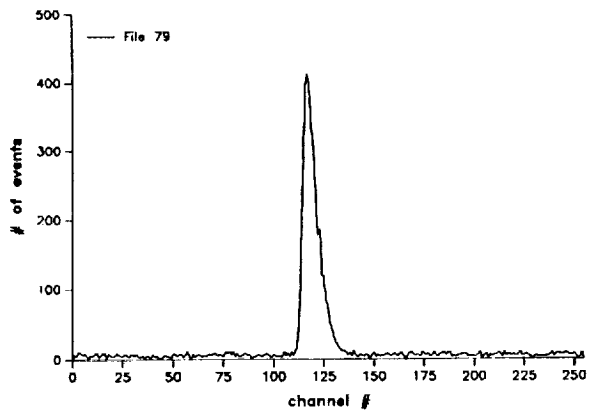

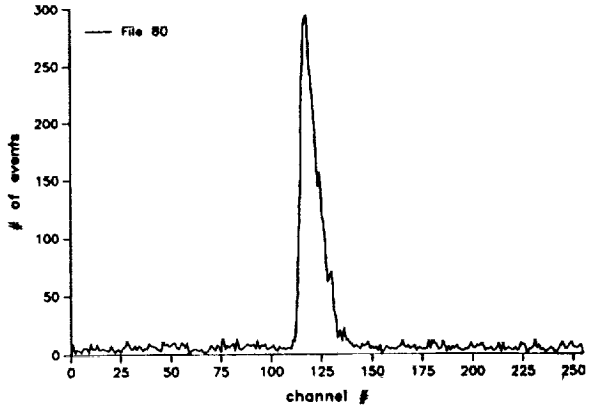

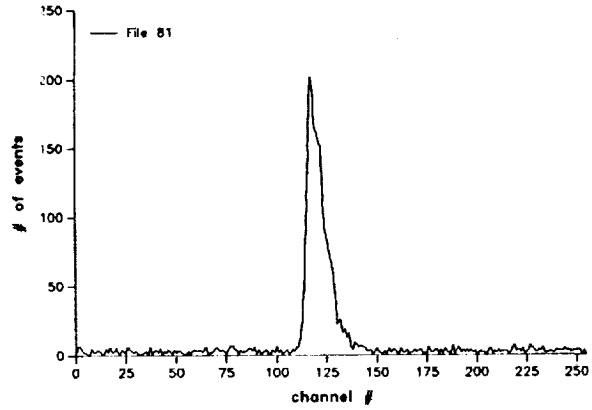

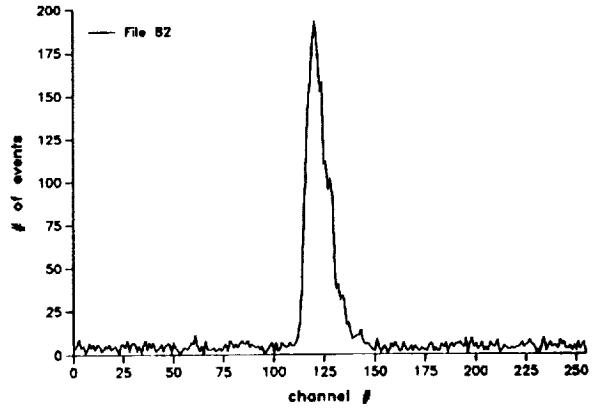

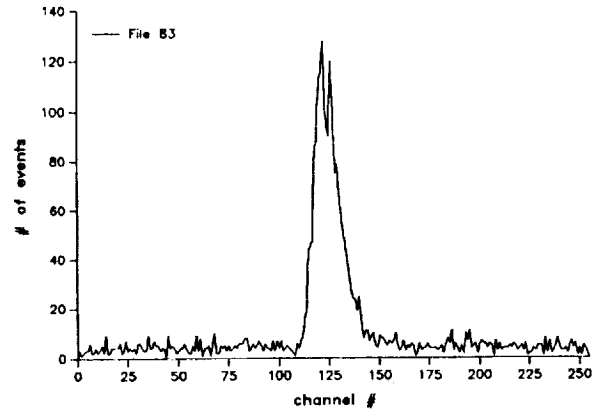

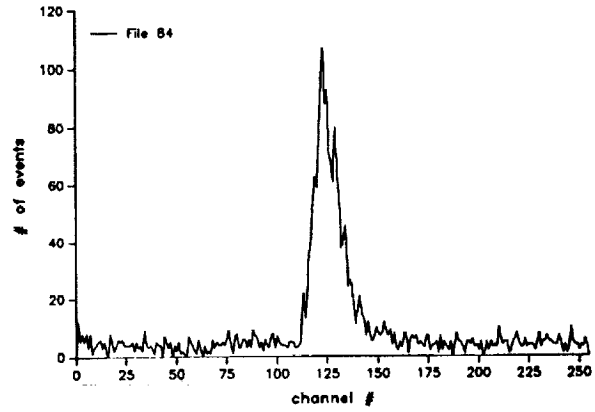

Figure 14: Continued

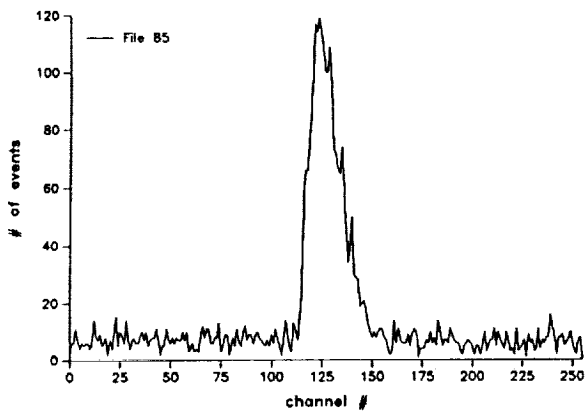

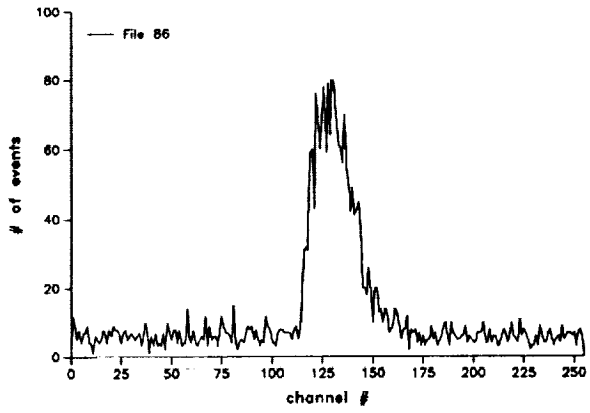

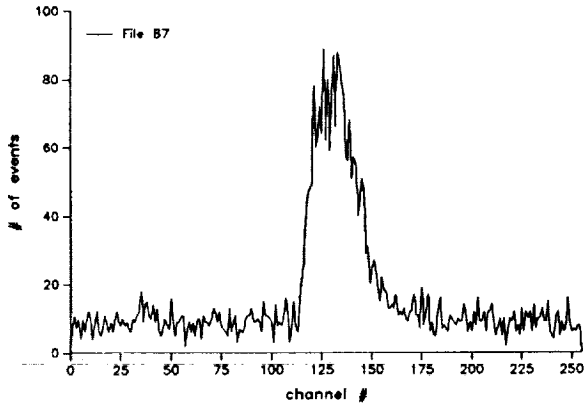

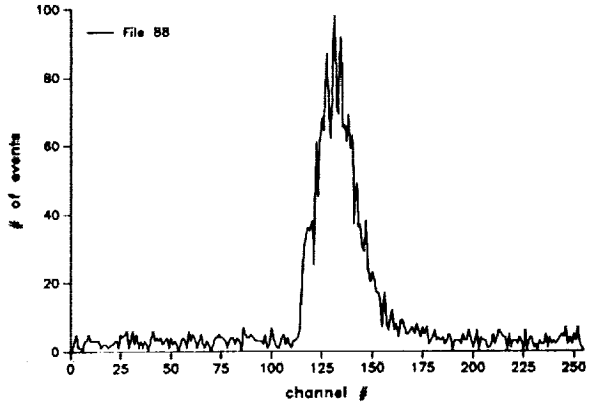

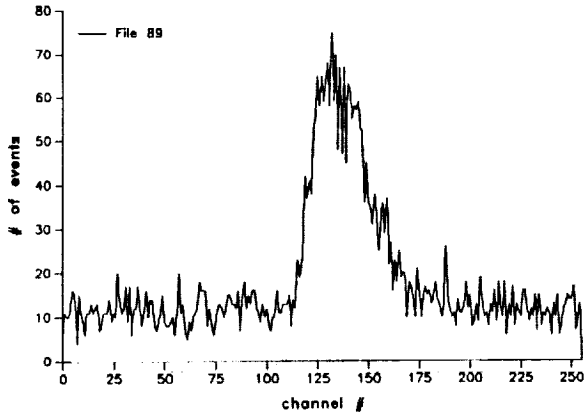

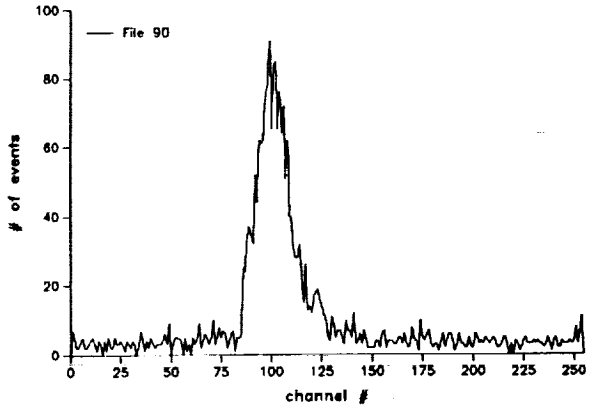

Figure 14: Continued

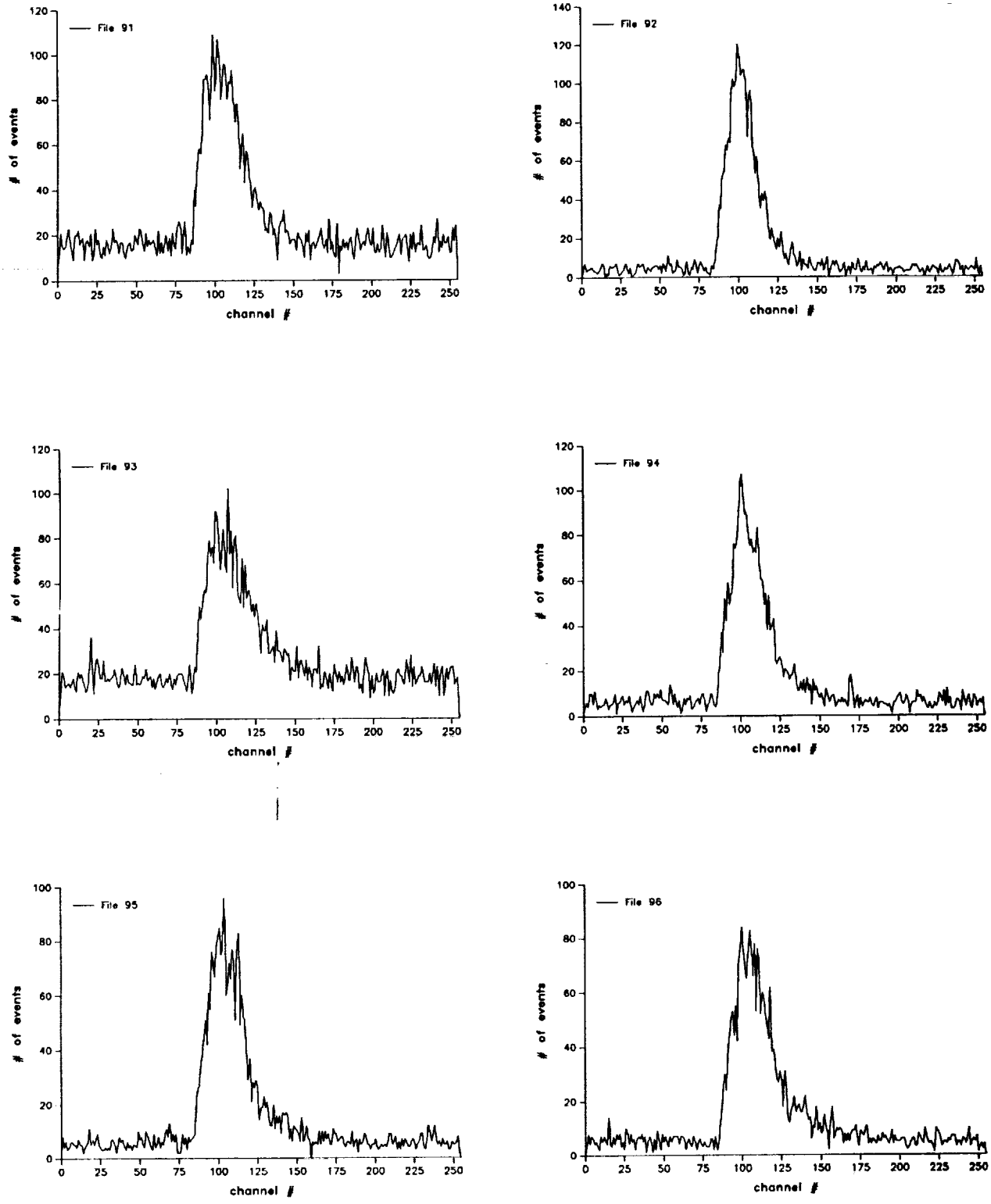

Figure 14: Continued

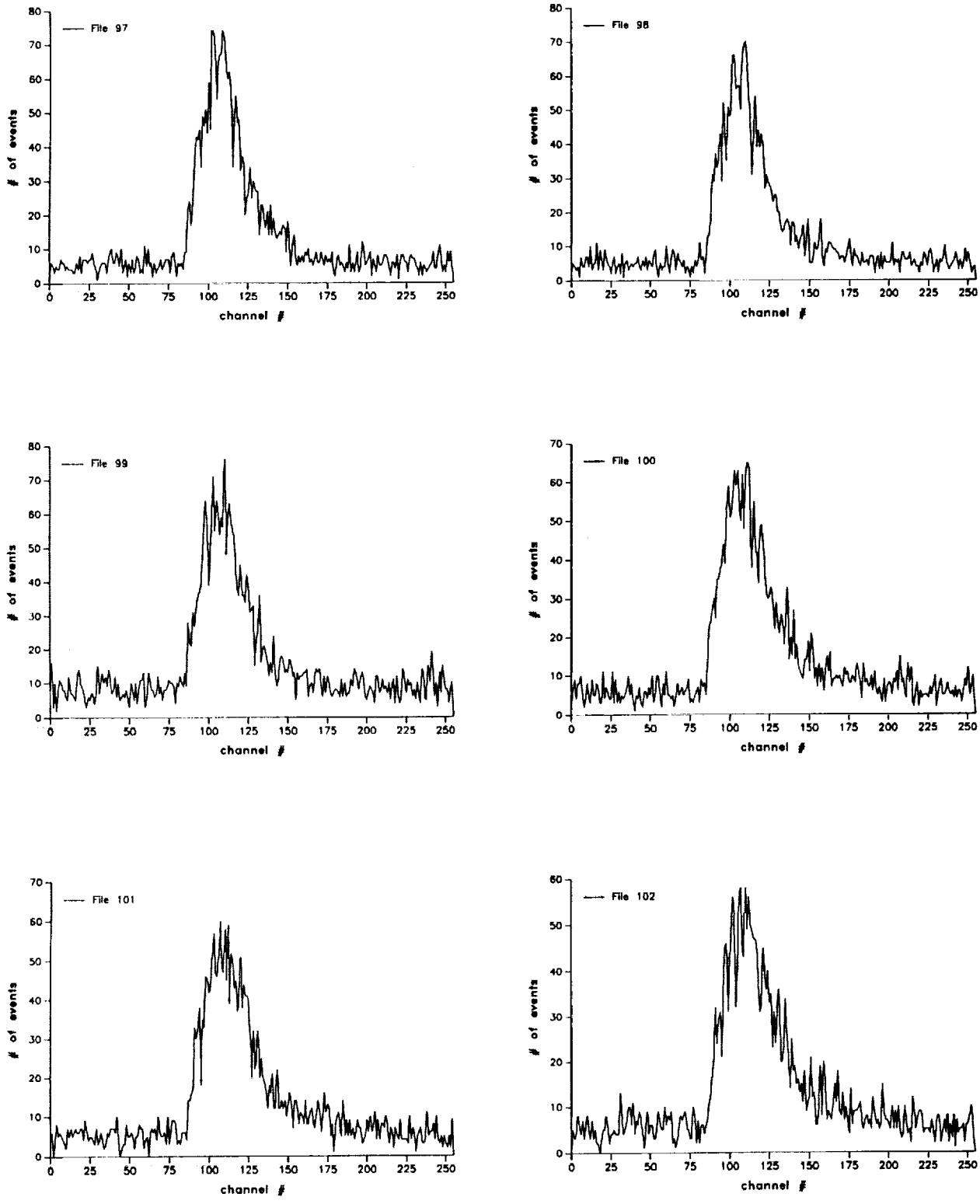

Figure 14: Continued

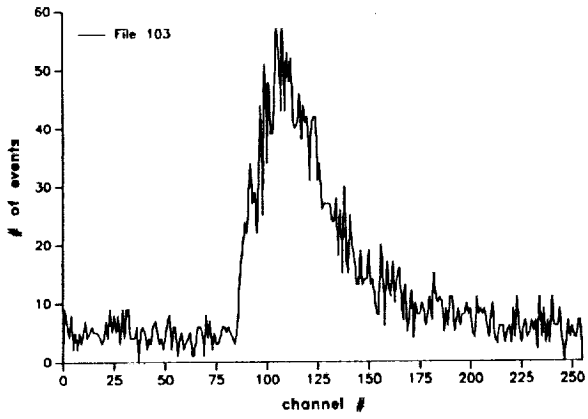

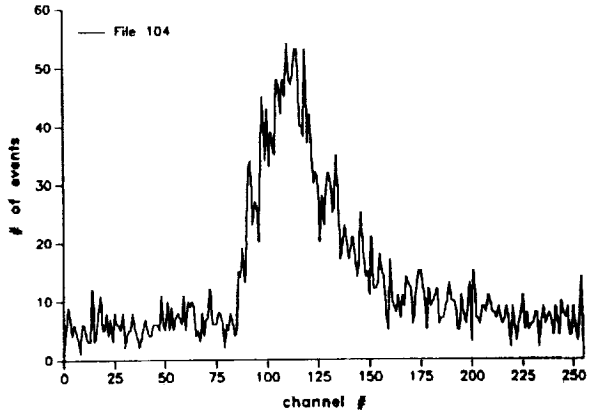

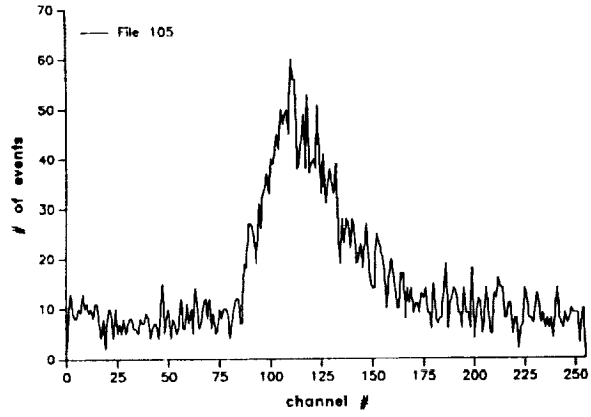

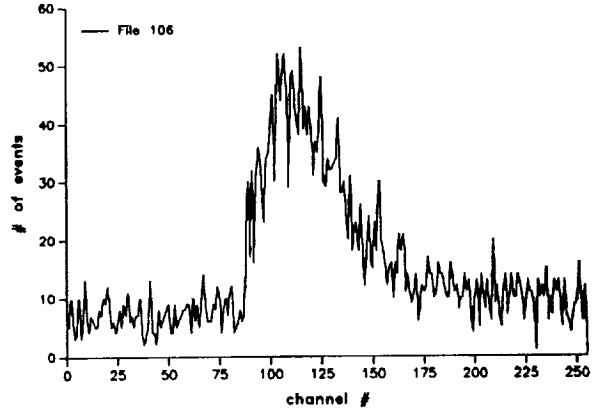

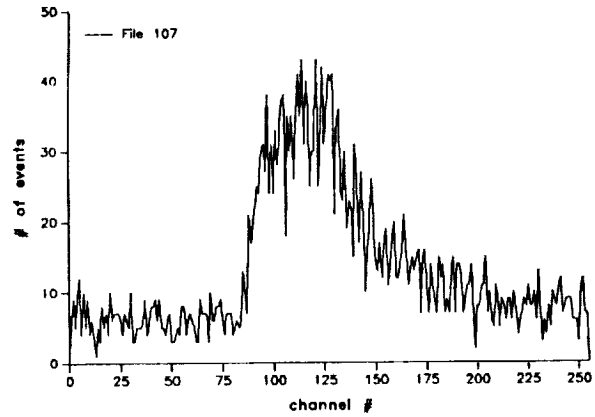

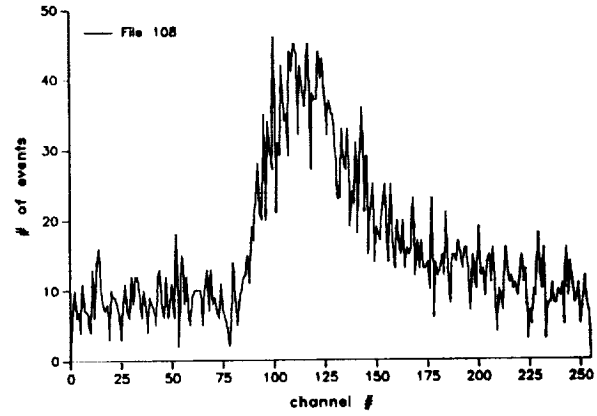

Figure 14: Continued

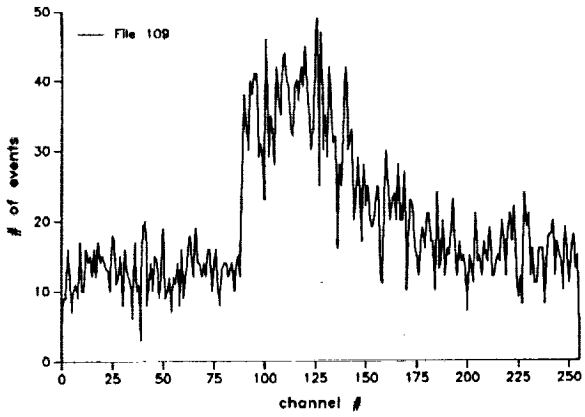

Figure 14: Concluded

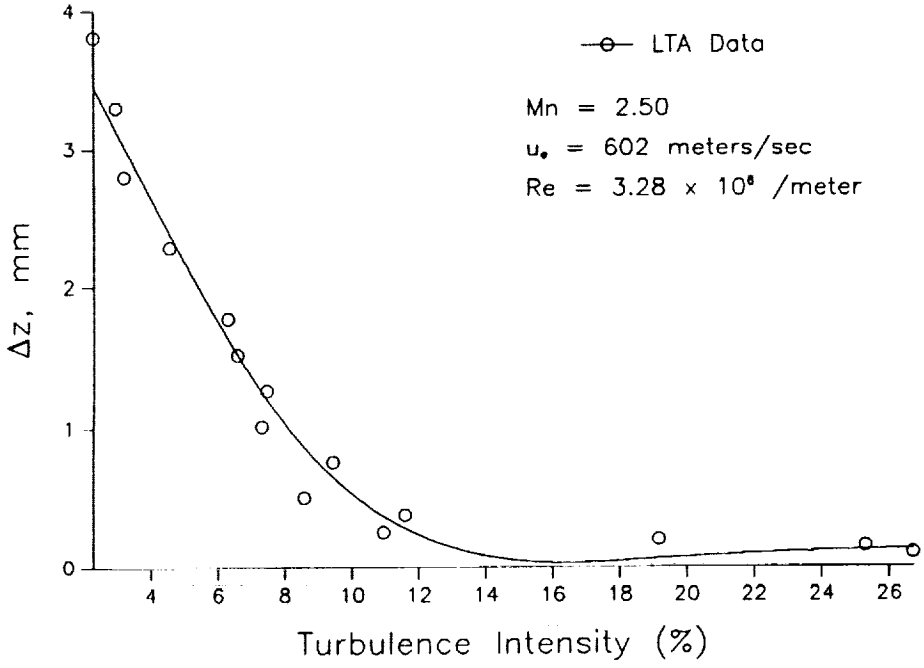

Figure 15: Turbulence Intensity Profile I

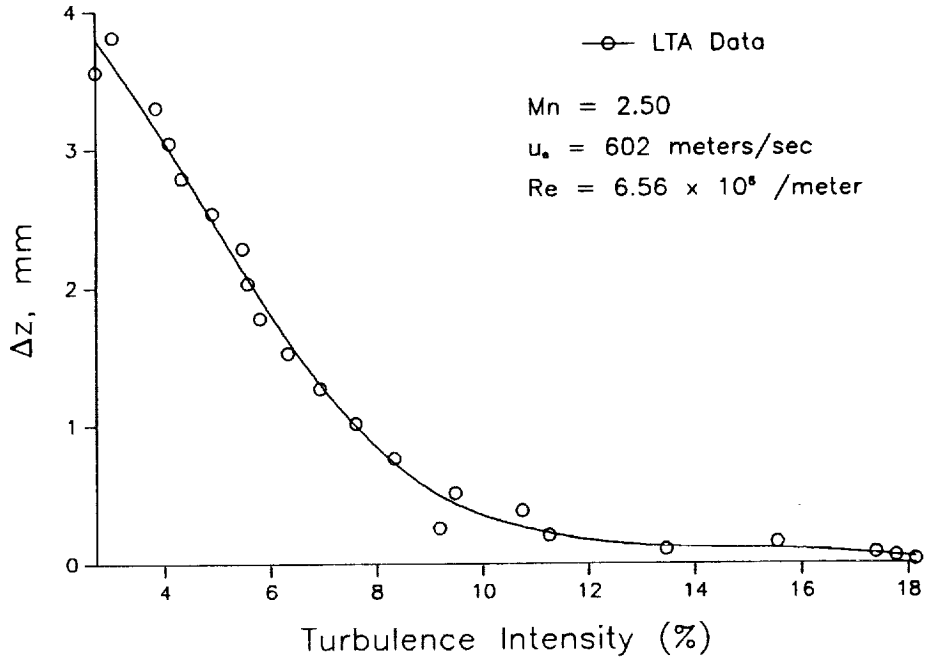

Figure 16: Turbulence Intensity Profile II

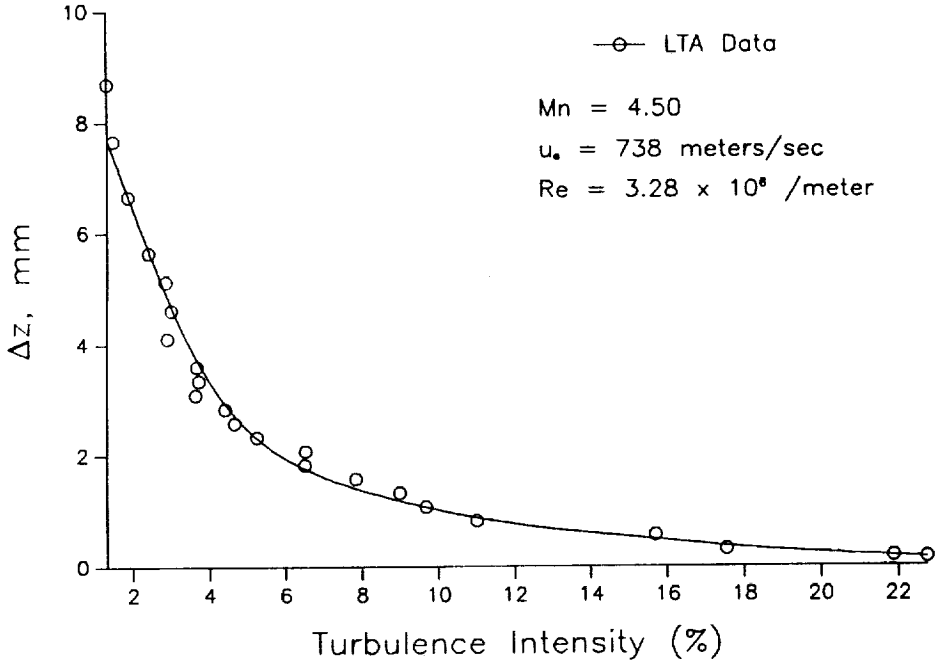

Figure 17: Turbulence Intensity Profile III

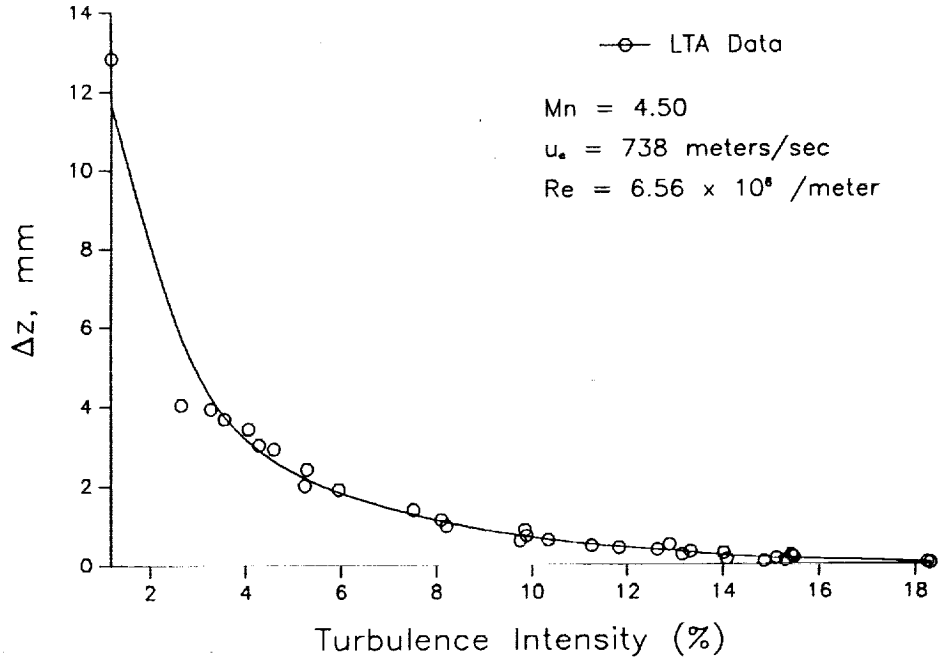

Figure 18: Turbulence Intensity Profile IV

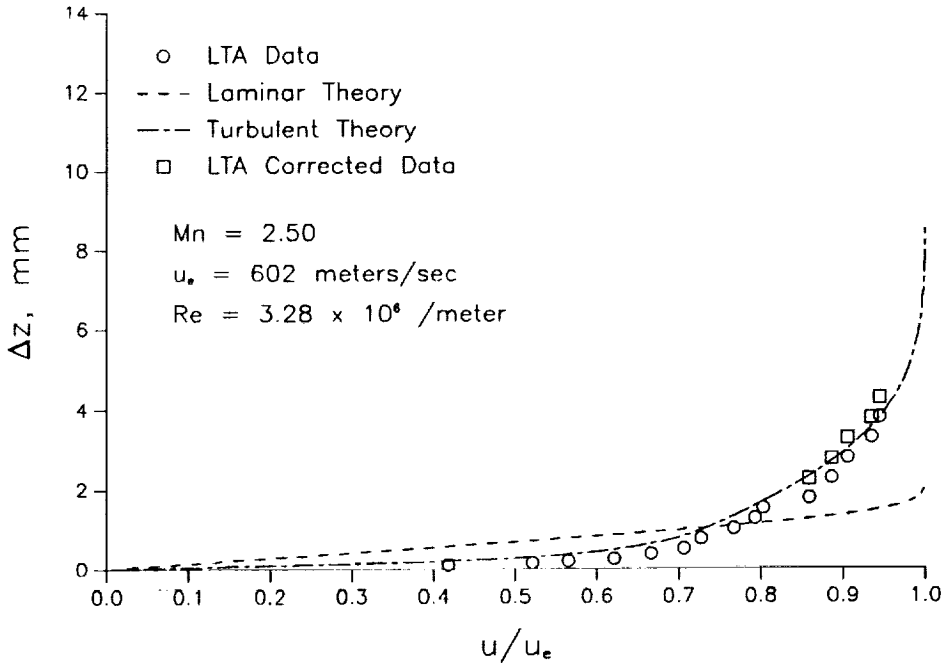

Figure 19: Boundary Layer Velocity Profile I

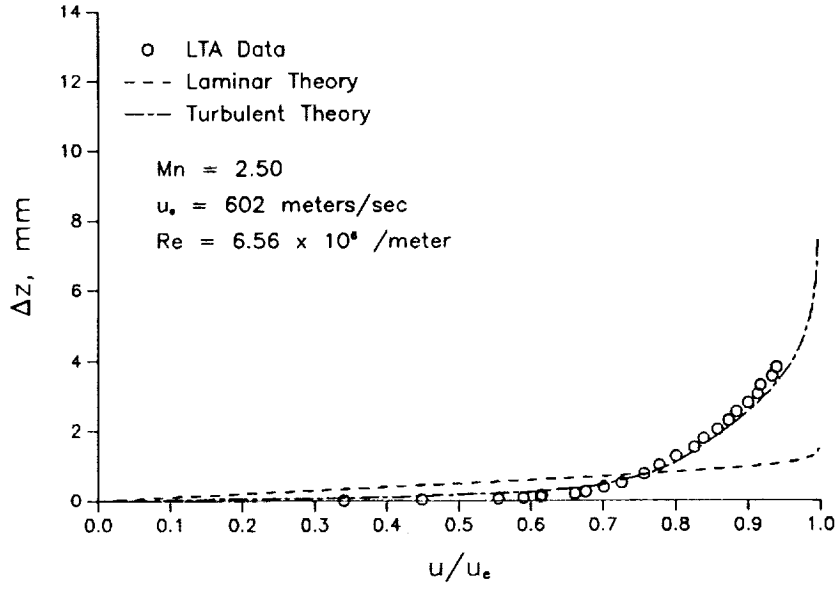

Figure 20: Boundary Layer Velocity Profile II

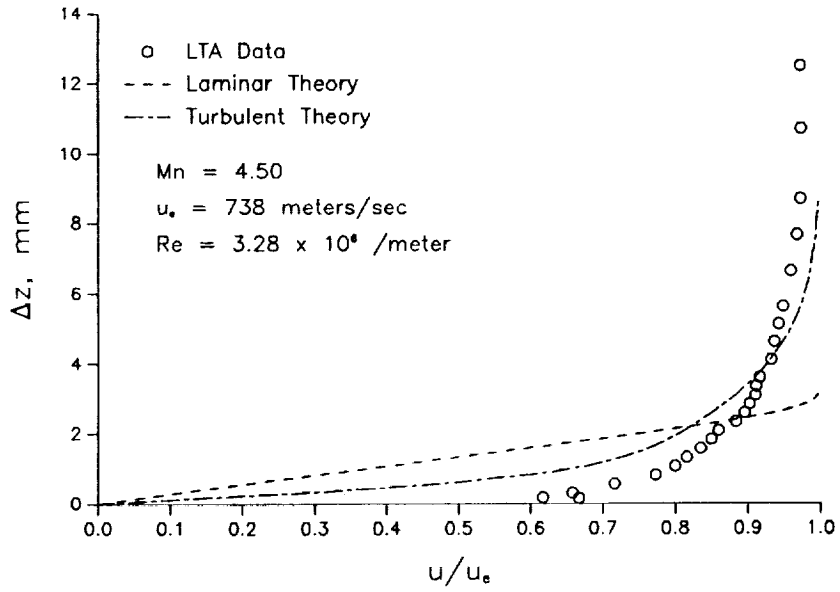

Figure 21: Boundary Layer Velocity Profile III

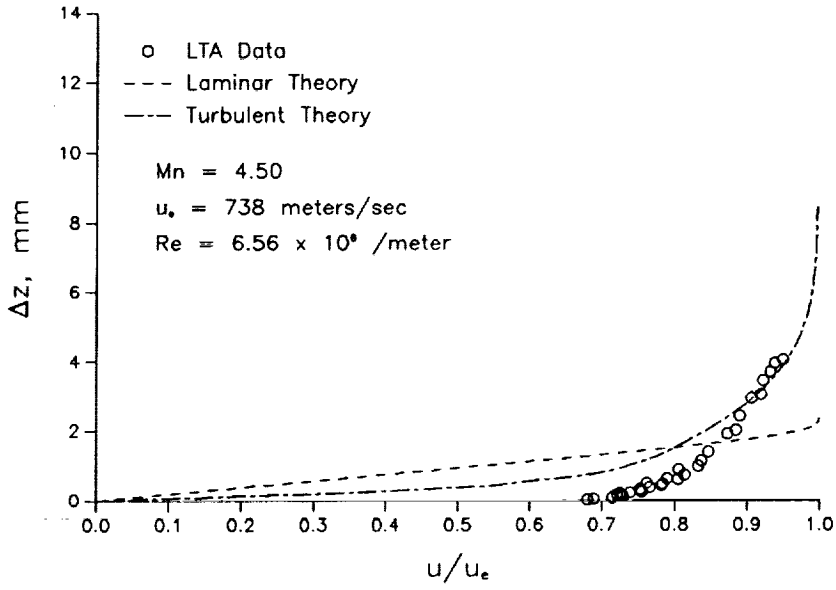

Figure 22: Boundary Layer Velocity Profile IV

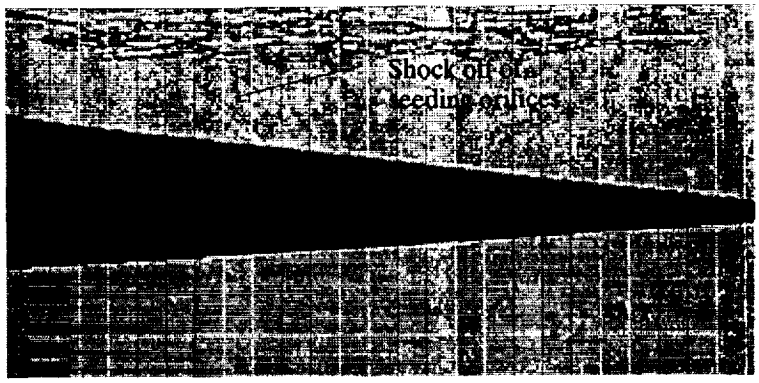

(a)

(b)

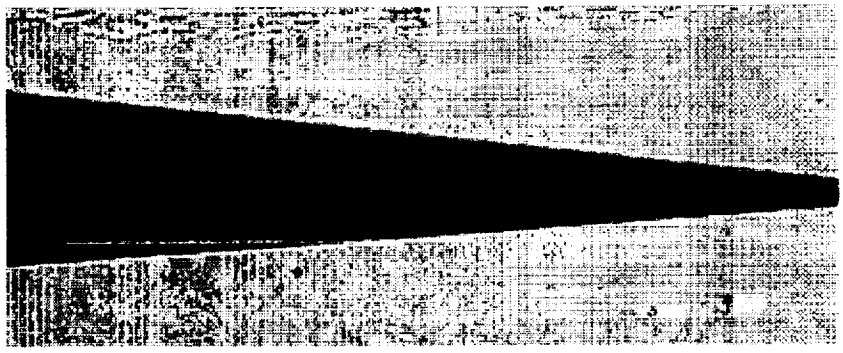

(c)

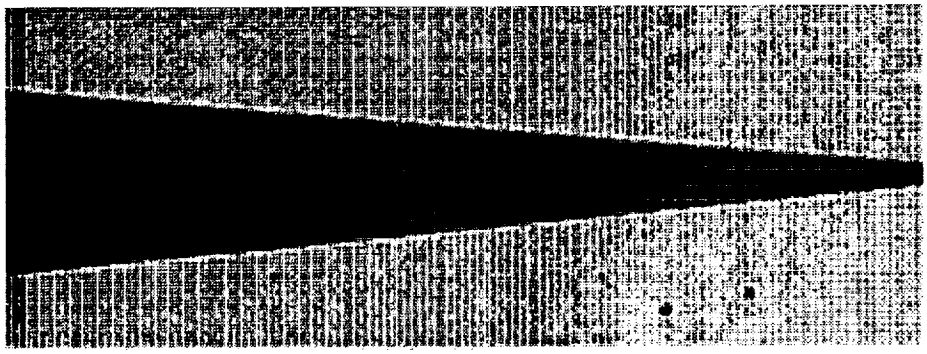

(d)

Figure 23: Shadowgraph Photos of Model
Mach # = 2.50 for all Photos
(a) Re = 3.281 x 10^6 / meter - Seeding On
(b) Re = 6.562 x 10^6 / meter - Seeding On
(c) Re = 3.281 x 10^6 / meter - Seeding Off
(d) Re = 6.562 x 10^6 / meter - Seeding Off

NASA National Aeronautics and Space Administration

Report Documentation Page

1. Report No.	2. Government Accession No.	3. Recipient's Catalog No.
NASA TM-102775		

4. Title and Subtitle
Laser Transit Anemometer Measurements on a Slender Cone in the Langley Unitary Plan Wind Tunnel

5. Report Date
December 1990

6. Performing Organization Code

7. Author(s)
William M. Humphreys, Jr., William W. Hunter, Jr.
Peter F. Covell, and Cecil E. Nichols, Jr.

8. Performing Organization Report No.

10. Work Unit No.
763-01-31-26

9. Performing Organization Name and Address
NASA Langley Research Center
Hampton, Virginia 23665-5225

11. Contract or Grant No.

13. Type of Report and Period Covered
Technical Memorandum

12. Sponsoring Agency Name and Address
National Aeronautics and Space Administration
Washington, DC 20546-0001

14. Sponsoring Agency Code

15. Supplementary Notes

16. Abstract A Laser Transit Anemometer (LTA) system has been used to probe the boundary layer on a slender (5 degree half angle) cone model in the Langley Unitary Plan Wind Tunnel. The anemometer system utilized a pair of laser beams with a diameter of 40 micrometers spaced 1230 micrometers apart to measure the transit times of ensembles of seeding particles using a cross-correlation technique. From these measurements, boundary layer profiles around the model were constructed and compared with CFD calculations. The measured boundary layer profiles representing the boundary layer velocity normalized to the edge velocity as a function of height above the model surface were collected with the model at zero angle of attack for four different flow conditions, and were collected in a vertical plane that bisected the model's longitudinal center line at a location 635 mm from the tip of the forebody cone. The results indicate an excellent ability of the LTA system to make velocity measurements deep into the boundary layer. However, because of disturbances in the flow field caused by onboard seeding, premature transition occurred implying that upstream seeding is mandatory if model flow field integrity is to be maintained. This paper presents a description and results of the flow field surveys.

17. Key Words (Suggested by Author(s))
Laser Transit Anemometer, LTA
Laser Velocimetry, LV
Boundary Layer Profiles
Wind Tunnel Flow Measurements

18. Distribution Statement
Unclassified - Unlimited
Subject Category - 35

19. Security Classif. (of this report)	20. Security Classif. (of this page)	21. No. of pages	22. Price
Unclassified	Unclassified	46	A03